KLF4 recruits SWI/SNF to increase chromatin accessibility and reprogram the endothelial enhancer landscape under laminar shear stress

Jan-Renier Moonen [1,2,3,4,9], James Chappell[5,9], Minyi Shi[5], Tsutomu Shinohara[1,2,3,4], Dan Li[1,2,3], Maxwell R. Mumbach[5,6], Fan Zhang [1,3], Ramesh V. Nair[7], Joseph Nasser[8], Daniel H. Mai [3], Shalina Taylor[1,2,3], Lingli Wang[1,2,3,4], Ross J. Metzger [1,3], Howard Y. Chang [5,6], Jesse M. Engreitz [4,5,8], Michael P. Snyder [2,5,7] & Marlene Rabinovitch [1,2,3,4] ✉

Physiologic laminar shear stress (LSS) induces an endothelial gene expression profile that is vasculo-protective. In this report, we delineate how LSS mediates changes in the epigenetic landscape to promote this beneficial response. We show that under LSS, KLF4 interacts with the SWI/SNF nucleosome remodeling complex to increase accessibility at enhancer sites that promote the expression of homeostatic endothelial genes. By combining molecular and computational approaches we discover enhancers that loop to promoters of KLF4- and LSS-responsive genes that stabilize endothelial cells and suppress inflammation, such as *BMPR2, SMAD5*, and *DUSP5*. By linking enhancers to genes that they regulate under physiologic LSS, our work establishes a foundation for interpreting how non-coding DNA variants in these regions might disrupt protective gene expression to influence vascular disease.

Regions of the arterial circulation exposed to uniform physiologic laminar shear stress (LSS) are associated with expression of vasculo-protective genes such as endothelial nitric oxide synthase (*NOS3*), whereas regions of low and disturbed shear stress, near arterial branches and bifurcations, are more prone to develop disease[1–5]. However, the nature and severity of vascular lesions depends on whether there are mitigating genetic and environmental factors that not only worsen the propensity to disease in vulnerable regions of the circulation, but also perturb the normal response to LSS.

Major effort has been directed at finding mechanosensing complexes in endothelial cells (EC) that respond to LSS to initiate a pattern of protective gene regulation that is altered in disease[6–8]. Krüppel-like factors (KLF) 2 and 4 have been identified as key transcription factors induced by LSS that control endothelial homeostatic gene regulation[9–13]. Beyond transcriptional activation at gene promoters, these factors might function as chromatin organizers to regulate genes by altering the chromatin landscape at distal enhancers. Knowing how the enhancer landscape changes in response to LSS provides a blue-

[1]Vera Moulton Wall Center for Pulmonary Vascular Diseases, Stanford University School of Medicine, Stanford, CA 94305, USA. [2]Stanford Cardiovascular Institute, Stanford University School of Medicine, Stanford, CA 94305, USA. [3]Department of Pediatrics, Stanford University School of Medicine, Stanford, CA 94305, USA. [4]BASE Initiative, Betty Irene Moore Children's Heart Center, Lucile Packard Children's Hospital, Stanford University School of Medicine, Stanford, CA 94305, USA. [5]Department of Genetics, Stanford University School of Medicine, Stanford, CA 94305, USA. [6]Center for Personal Dynamic Regulomes, Stanford University School of Medicine, Stanford, CA 94305, USA. [7]Stanford Center for Genomics and Personalized Medicine, Stanford University School of Medicine, Stanford, CA 94305, USA. [8]Broad Institute of MIT and Harvard, Cambridge, MA 02142, USA. [9]These authors contributed equally: Jan-Renier Moonen, James Chappell. ✉e-mail: marlener@stanford.edu

print that will better inform how variants in non-coding DNA can influence vascular diseases, including pulmonary arterial hypertension (PAH), which is characterized by progressive occlusion of distal pulmonary arteries[14,15]. Pathogenic gene variants in *BMPR2* are the most common genetic risk factor for PAH, but have been associated with only 15% of patients with the non-familial form of the disease[16,17], suggesting that variants in non-coding DNA regions might contribute to a reduction in BMPR2 levels or in downstream effectors of BMPR2 mediated gene regulation in patients with PAH.

Whereas variants in coding and proximal regulatory DNA regions can be readily related to dysfunction of a particular disease-causing gene, ascribing variants in distal non-coding regions to genes related to vascular disease has been more elusive. New bioinformatic approaches are overcoming this hurdle. For example, a variant in a distal enhancer that targets endothelin-1 was recently linked to five vascular diseases[18]. With more effort directed at whole genome sequencing in cohorts of patients such as those with PAH, establishing the functional significance of variants in non-coding DNA has become increasingly important. Moreover, variants identified in enhancers that are active under physiologic LSS might have the greatest adverse impact on gene regulation.

We, therefore, sought to map the enhancer landscape of pulmonary artery EC (PAEC) exposed to LSS by first relating changes in chromatin accessibility, determined by ATAC-Seq, to gene expression, assessed by RNA-Seq. We find an overall increase in chromatin accessibility, coinciding with the induction of protective genes and suppression of disease-related genes. Motif analyses of differentially accessible regions (DAR) reveal enrichment for KLF binding sites in regions with increased accessibility under LSS, which we confirm by KLF4 ChIP-Seq. We demonstrate, using KLF gain-and-loss-of-function experiments, that KLF is required to mediate chromatin accessibility changes at proximal and distal sites, adding to the known role for KLF in transcriptional activation of flow responsive genes.

Consistent with this finding, we identify components of the SWItch/Sucrose Non-Fermentable (SWI/SNF) nucleosome remodeling complex that are recruited by KLF4 and required for KLF-mediated gene regulation. H3K27ac HiC Chromatin Immunoprecipitation (HiChIP)[19,20] shows increased enhancer looping to LSS-responsive genes, often spanning multiple genes. Application of the Activity-by-Contact (ABC) algorithm[21], which identifies regulatory elements of specific genes based upon chromatin accessibility and H3K27ac levels, predicts more than 70% of genes differentially expressed under LSS to be regulated by KLF4. These data provide a blueprint of the endothelial enhancer landscape under physiologic LSS, which informs future studies on how variants in non-coding DNA might impair protective gene expression and promote vascular disease.

Results

LSS alters chromatin accessibility, increasing the expression of vasculo-protective genes

Genome-wide changes in chromatin accessibility and gene expression were studied by ATAC-Seq and RNA-Seq in PAEC exposed to a physiologic level of 15 dyn/cm² of LSS[5,22] for 24 h (Fig. 1a). Exposure to LSS increased accessibility of 4699 genomic regions while 2191 regions showed a loss of accessibility compared to PAEC cultured under static conditions (ST) (Fig. 1b). Whereas a subset of these DAR contains gene promoters, most DAR are located in introns or at intergenic sites (Fig. 1c). When assigning DAR to their nearest genes, we found that the majority of DAR are located within 100 Kb of a transcription start site (Fig. 1d). We then performed motif enrichment analyses on all DAR. In regions with increased accessibility under LSS, we found enrichment for motifs that are recognized by members of the KLF family (77% of DAR, $P = 1E-227$), while activator protein-1 (AP1) motifs were most enriched in regions where accessibility was lost (58% of DAR, $P = 1E-205$). Motifs for E26 transformation-specific (ETS) family members

were present in about 80% of DAR under both LSS and static culture conditions, which is in line with previous reports indicating ETS as indispensable for endothelial gene regulation[23,24] (Fig. 1e and Supplementary Fig. 1).

Immunofluorescence was next applied to assess nuclear expression of these transcription factor families under LSS and ST conditions, which confirmed the increased expression of KLF4 with LSS, while the AP1 family member activating transcription factor-2 (ATF2), which is increased in endothelial cells in atherosclerotic lesions[25], was increased under static conditions. ETS1 was constitutively expressed under both conditions (Fig. 1f).

To relate chromatin accessibility changes to altered gene expression, we performed RNA-Seq of PAEC cultured under identical conditions. Induction of the LSS-responsive transcription factors KLF2 and KLF4 was confirmed by RNA-Seq and RT-qPCR (Supplementary Fig. 2a, b). We observed 720 and 663 genes significantly up- or downregulated, respectively, with LSS compared to ST conditions (Fig. 1g). Exposure to LSS resulted in induction of a quiescent vasculo-protective gene expression profile, as evident in enrichment for genes related to blood vessel development, improved barrier function and enhanced cell-matrix interaction (Fig. 1h, upper panel). In contrast, the gene expression profile of PAEC cultured under ST conditions is typical of a more activated and proliferative phenotype, including genes that promote cell migration, cell cycle molecules, and genes related to oxidative stress (Fig. 1h, lower panel). We found that the gene expression profile of PAEC cultured under static conditions is very similar to that of PAEC exposed to +/−3 dyn/cm² of oscillatory shear stress (OSS) (Supplementary Fig. 2c–e) which agrees with previous observations by Qiao et al.[26].

When relating LSS-mediated DAR to their nearest gene, we found a positive correlation between chromatin accessibility changes and altered gene expression ($r = 0.41$, $P < 0.0001$) (Fig. 1i). Differentially expressed genes (DEG) associated with proximal accessibility changes were enriched for pathways related to extracellular matrix components, e.g., elastic fiber formation (*ELN*, *FBN1*, and *FBLN2*), collagen formation (*COL3A1*, *COL4A1*, and *COL5A2*), laminin interactions (*LAMA5*, *ITGBA6*, *and ITGB4*), and chondroitin sulfate/dermatan sulfate metabolism (*HYAL1*, *VCAN*, *GBE1*, *CHST3*, and *CHST11*), as well as matrix metalloproteinases and disintegrins (*MMP15*, *MMP28*, *ADAM15*, *ADAMTS1*, and *ADAMTS9*) and Insulin-like growth factor and Notch signaling components (*IGFBP5*, *HES1*, *JAG1*, and *DLL1*) (Supplementary Fig. 3a, b).

DEG without proximal accessibility changes were enriched for pathways related to suppression of cell proliferation, e.g., a decrease in nucleosome assembly genes (*CENPA*, *CENPM*, *CENPN*, and *CENPP*), multiple histone genes, and suppression of genes related to the resolution of sister chromatids (*PLK1* and *AURKB*), as well as several mini-chromosome maintenance (MCM) genes that are involved in the initiation of eukaryotic genome replication (*MCM2*, *MCM4*, *MCM5*, and *MCM7*) (Supplementary Fig. 3a, c).

KLF regulates chromatin accessibility of vasculoprotective genes under LSS

To determine whether KLF regulates changes in chromatin accessibility under LSS, we performed ATAC-Seq under conditions of KLF gain- or loss-of-function. For gain-of-function studies, we transduced PAEC with an adenoviral vector encoding a constitutively active mutant of mitogen-activated protein kinase kinase 5 (caMEK5), which leads to phosphoactivation of signal-regulated kinase 5 (ERK5) and the induction of KLF2 and KLF4[27,28]. PAEC transduced with caMEK5 showed a 14- and 22-fold increase in expression of KLF2 and KLF4, respectively, compared to controls transduced with a vector encoding green fluorescent protein (GFP) (Supplementary Fig. 4a) which is similar to what we observed in wildtype cells exposed to LSS (Supplementary Fig. 2a, b). Almost half of the DAR previously
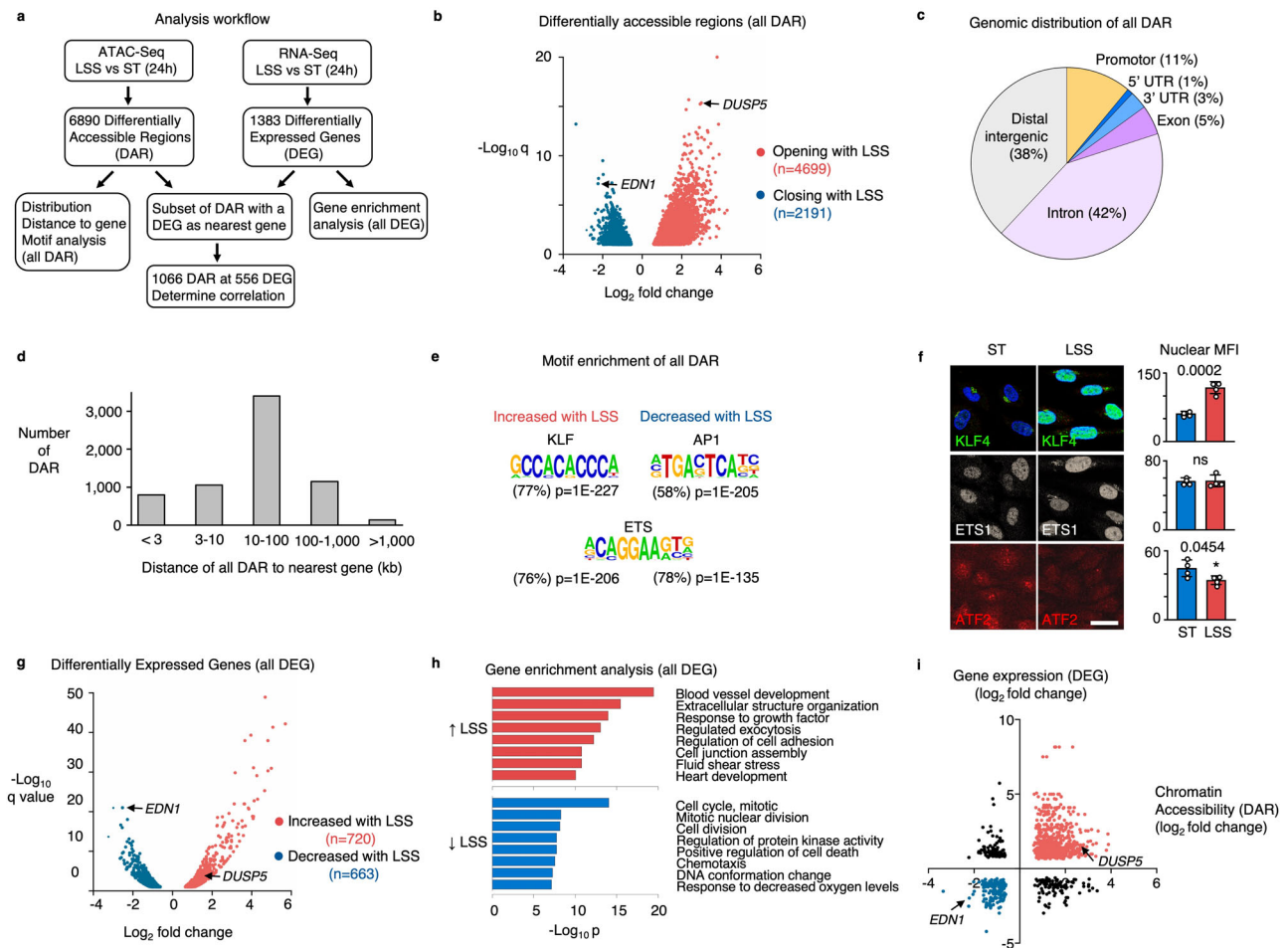
Fig. 1 | Laminar shear stress increases chromatin accessibility and vasculoprotective gene expression. a Schematic illustration of the workflow and analysis. **b** Volcano plot showing the differentially accessible regions (DAR) determined by ATAC-Seq in PAEC that were exposed to 15 dyn/cm^2 of LSS for 24 h vs static controls. Each dot represents a DAR. Red dots are DAR with increased accessibility, blue dots are DAR with decreased accessibility under LSS. Highlighted genes are described in subsequent sections. $n = 3$ experimental replicates. P values were determined by a two-tailed Wald test with Benjamini–Hochberg adjustment. **c** Pie chart showing the annotation of DAR peaks, analyzed using Homer. **d** Bar graphs showing the distance of DAR to its nearest gene, analyzed using Homer. **e** Motif enrichment of DAR with increased or decreased accessibility with LSS, analyzed using Homer. P values were determined by binomial test. **f** Representative immunofluorescent images (left) with quantitation on the right, of PAEC that were exposed to 15 dyn/cm^2 of LSS for 24 h vs static controls (ST), showing the nuclear expression of KLF4 (green); ETS1 (gray), and ATF2 (red). Nuclei were stained with DAPI, (blue). $n = 4$ experimental replicates. Bars indicate mean ± s.e.m. P values were determined by Student's two-tailed t-test. ns: not significant. Source data are provided as a Source Data file. Scale bar, 20 μm. **g** Volcano plot showing the differentially expressed genes (DEG) determined by RNA-Seq in PAEC exposed to 15 dyn/cm^2 of LSS for 24 h vs Static controls. Each dot represents a gene. Red dots are DEG with increased expression under LSS, blue dots are DEG with decreased expression under LSS. Highlighted genes are described in subsequent sections. $n = 2$ experimental replicates. P values were determined by a two-tailed Wald test with Benjamini–Hochberg adjustment. **h** Gene enrichment analysis using Metascape of genes that are induced by LSS (red bars) and genes that are repressed by LSS (blue bars). P values were determined by a one-tailed hypergeometric test with Benjamin-Hochberg adjustment. **i** Scatterplot showing a positive correlation of accessibility changes with the expression of its nearest differentially expressed gene. Highlighted genes are described in subsequent sections. $r = 0.41$ with $P < 0.0001$ determined by two-tailed Pearson R test.

identified under LSS versus ST were also differentially accessible in caMEK5-transduced PAEC compared to GFP controls ($n = 3211/6890$), and accessibility changes were highly correlated ($r = 0.89$, $P < 0.0001$) (Fig. 2a, left panel). When plotting the correlation of all LSS vs ST DAR with accessibility changes in caMEK5-transduced PAEC at those sites, we found a correlation of $r = 0.78$ ($P < 0.0001$) (Supplementary Fig. 4b), indicating that activation of ERK5 and induction of KLF2/4 as previously described with LSS[28] is largely responsible for the changes in chromatin accessibility. Similarly, the gene expression changes in caMEK5-transduced cells assessed by RNA-Seq strongly correlated with those observed with LSS ($n = 1164$, $r = 0.82$, $P < 0.0001$). (Fig. 2a, right panel).

To further corroborate that KLF is required to alter chromatin accessibility under LSS, we performed loss-of-function experiments using siRNA simultaneously targeting KLF2 and KLF4. KLF siRNA

reduced KLF2 and KLF4 gene expression levels under LSS by 79.7% and 69.8%, respectively (Supplementary Fig. 4c). We note that this still corresponds to 4.9- and 7.8-fold higher gene expression compared to ST conditions. KLF2/4 protein expression was reduced by 60% (Supplementary Fig. 4d). A subset of regions did not show the increase in accessibility that we previously observed with LSS (Fig. 2b, left panel) which coincided with a subset of genes not being induced (Fig. 2b, right panel). When plotting all LSS vs ST DAR with accessibility changes in KLF RNAi-treated PAEC at those sites, we found a correlation of $r = -0.73$ ($P < 0.0001$) (Supplementary Fig. 4e).

We observed a modest increase in accessibility at the promoter regions of a known endothelial flow responsive gene and KLF4 target, *NOS3*[11] (Supplementary Fig. 5), as these sites were also highly accessible under static conditions. We also identified prominent DAR associated with flow-responsive genes. An example is *DUSP5*, a dual specificity
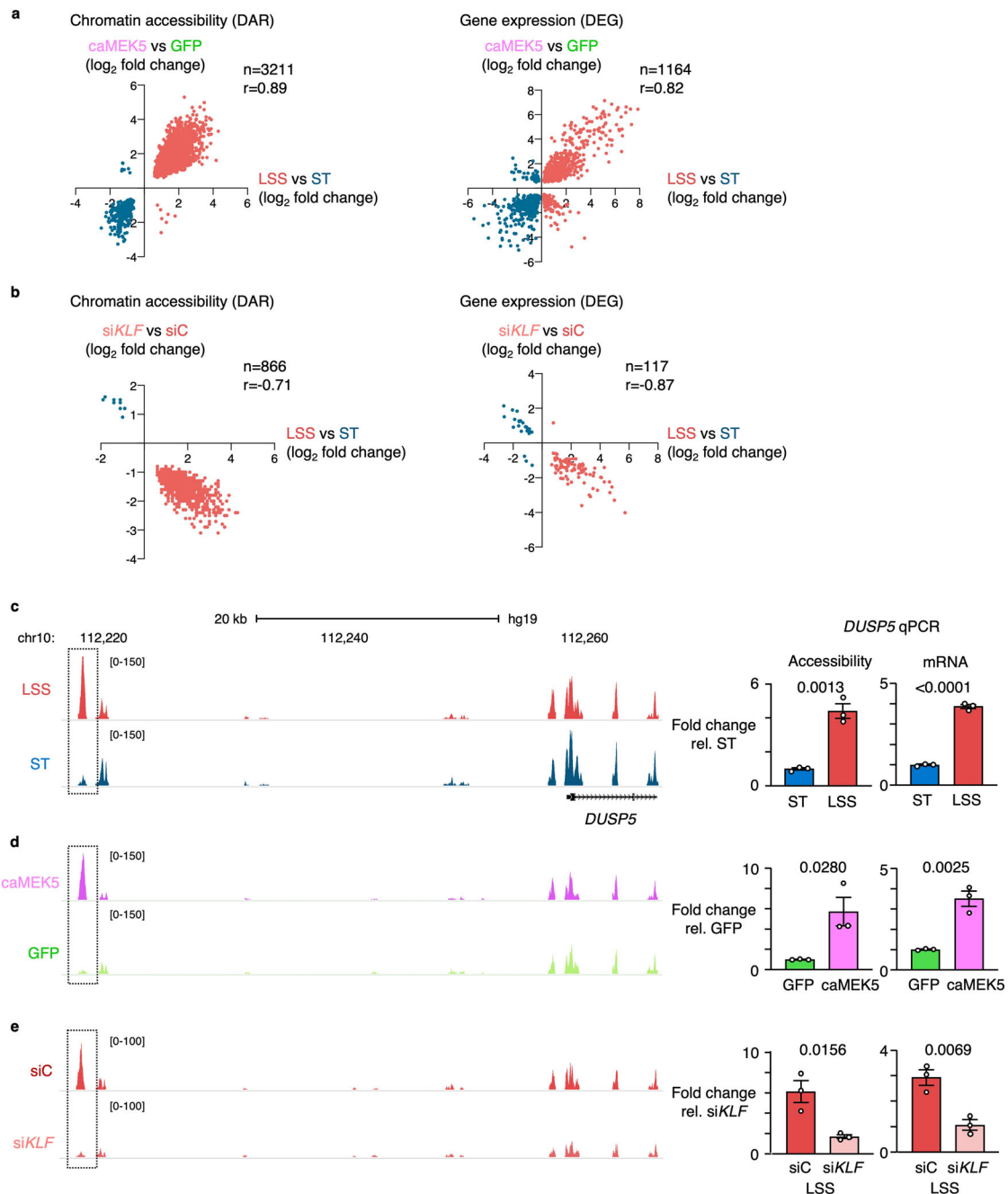
Fig. 2 | KLF regulates chromatin accessibility of vasculo-protective genes under LSS. a PAEC were transduced overnight with adenoviral vectors encoding caMEK5 or GFP as control. Ninety hours after transduction, chromatin accessibility changes were analyzed by ATAC-Seq and gene expression changes by RNA-Seq. Scatterplots show the correlation between changes in chromatin accessibility (left panel) and gene expression (right panel) in caMEK5 transduced PAEC compared to PAEC exposed to LSS. $n = 3$ experimental replicates. Indicated values were calculated by a two-tailed Pearson R test, with $P < 0.0001$. Each dot represents a differentially accessible region (left panel) or differentially expressed gene (right panel). b PAEC were treated with siRNA targeting KLF2 and KLF4 (siKLF), or non-targeting controls (SiC), 24 h prior to exposing the cells to 15 dyn/cm² of LSS vs ST conditions for an additional 24 h. Chromatin accessibility changes were analyzed by ATAC-Seq and gene expression changes by RNA-Seq. Scatterplots show the correlation between changes in chromatin accessibility (left panel) and gene expression (right panel) in siKLF treated cells compared to untreated PAEC exposed to 15 dyn/cm² of LSS for 24 h. $n = 3$ experimental replicates. Indicated values were calculated by a two-tailed Pearson R test, with $P < 0.0001$. Each dot represents a DAR (left panel) or DEG (right panel). c ATAC-Seq tracks showing a DAR upstream of DUSP5 with increased accessibility under LSS vs ST control (left panel). Bar graphs showing the ATAC-qPCR analysis of the DUSP5 DAR, and of DUSP5 mRNA transcript levels by RT-qPCR (right panel). d ATAC-Seq tracks showing increased accessibility of the DAR upstream of DUSP5 in PAEC transduced with caMEK5 vs GFP controls. Bar graphs of the ATAC-qPCR and RT-qPCR analyses of caMEK5 transduced PAEC as described above (right panel). e ATAC-Seq tracks of PAEC treated with siKLF as described above (left panel). Bar graphs of the ATAC-qPCR and RT-qPCR analyses of siKLF treated PAEC (right panel). For c–e, $n = 3$ experimental replicates. qPCR data are shown as the mean +/− s.e.m. P values were determined by Student's two-tailed t-test. Source data are provided as a Source Data file.

phosphatase that inhibits ERK1/2 signaling[29]. ATAC-Seq identified a potential regulatory DAR located 39 Kb upstream of the *DUSP5* transcription start site (TSS). ATAC-qPCR confirmed the increased accessibility at that site with LSS, which coincided with higher *DUSP5* mRNA transcript levels (Fig. 2c). When investigating a broader region surrounding the *DUSP5* locus, many sites where similarly accessible under LSS versus ST conditions (Supplementary Fig. 6). caMEK5 transduced cells had increased accessibility at the regulatory region located 39 kb upstream of the TSS, which was confirmed by qPCR (Fig. 2d and Supplementary Fig. 6). Upon silencing of KLF2 and KLF4 by RNAi prior to exposure to LSS, neither an increase in this DAR, nor the induction of *DUSP5* gene expression were observed (Fig. 2e and Supplementary Fig. 6). DUSP5 loss-of-function experiments revealed that DUSP5 is responsible for repressing multiple chemoattractant, antiviral and interferon genes under LSS (Supplementary Fig. 7). In addition to *DUSP5*, we investigated other DEG that had DAR associated with it, such as those illustrated in Supplementary Fig. 3. For *COL3A1* and *DLL1*, we found a single DAR proximal to the gene TSS. For *ITGB4*, *ITGA6* and *HYAL1*, we found multiple DAR near the TSS (Supplementary Fig. 8). As we observed at the *DUSP5* locus, across a broader region, many sites

were similarly accessible under LSS and ST conditions, reinforcing that the DAR represent flow-responsive regulatory sites. Overall, we found lower intensity of ATAC-Seq peaks with KLF siRNA, compared to untreated PAEC exposed to LSS or those transduced with caMEK5, likely for technical reasons.

KLF4 interacts with the SWI/SNF nucleosome remodeling complex to increase chromatin accessibility

Having established that loss of KLF reduces chromatin accessibility, we next sought to identify a chromatin remodeler with which it might interact to exert these changes. We transduced PAEC with an adeno-viral vector encoding a Flag-tagged mutant of KLF4 or with a GFP vector as control, and performed affinity purification followed by mass spectrometry (AP-MS) using anti-KLF and anti-Flag antibodies. We found, with both antibodies, that KLF4 co-purified with ten components of the SWI/SNF nucleosome remodeling complex, including the ATP-dependent helicase Brahma-Related Gene 1 (BRG1), also known as SMARCA4, and the invariable core subunit SMARCC2 (Fig. 3a). In addition to the SWI/SNF complex, we found KLF4 co-purified with several other chromatin remodelers that enhance chromatin
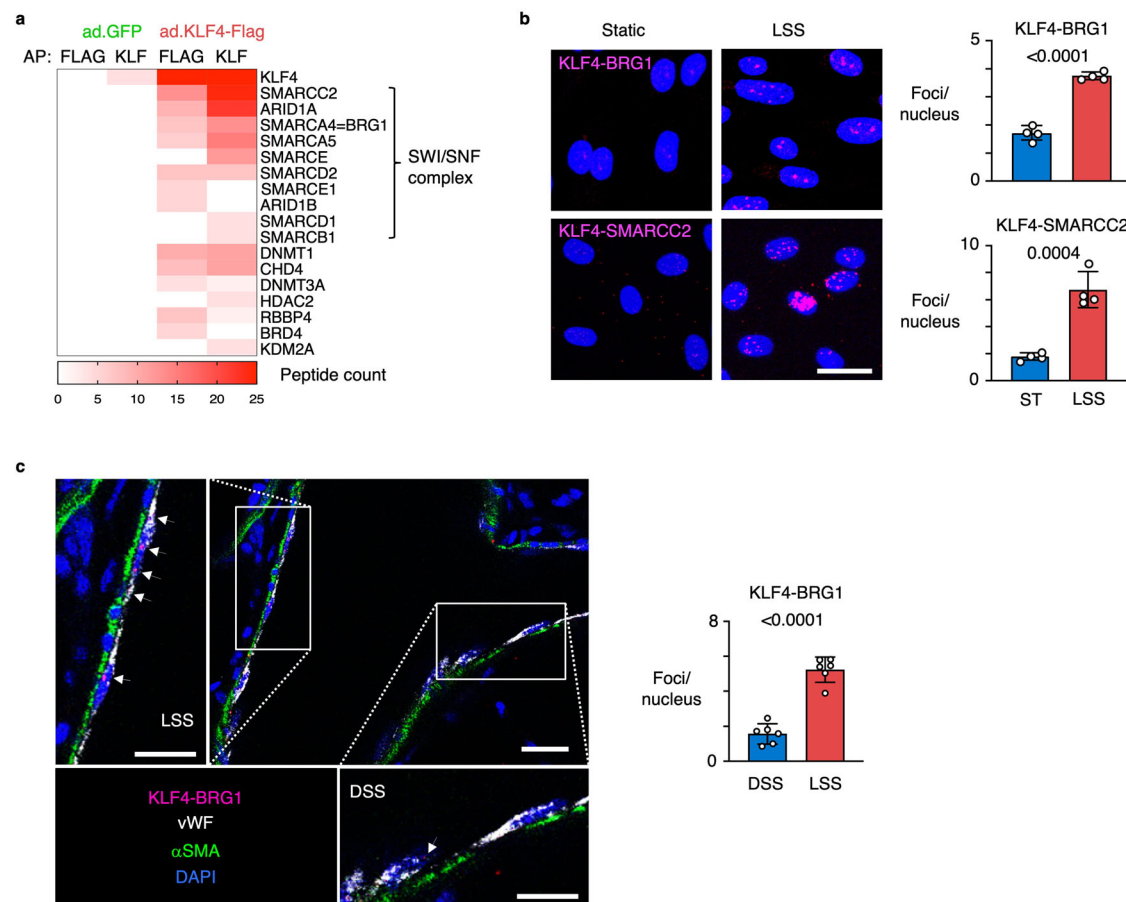

Fig. 3 | KLF4 interacts with the SWI-SNF nucleosome remodeling complex to increase chromatin accessibility. a Heatmap showing the spectral counts obtained by Affinity Purification followed by Mass Spectrometry (AP-MS) of PAEC transduced with adenoviral vectors encoding a Flag-tagged mutant of KLF4 or GFP control. AP was performed using anti-Flag antibodies (FLAG) and anti-KLF antibodies (KLF). Proteins were inferred from the peptides against the human UniProt using an FDR of 1%. *n* = 2 experimental replicates. **b** Representative images of Proximity Ligation Assays (PLA) (left panel) of PAEC exposed to 15 dyn/cm² of LSS or ST conditions for 24 h, show an interaction of KLF4 with BRG1 and SMARCC2 under LSS (magenta). Nuclei were stained with DAPI (blue). Number of foci per nucleus were quantified in 10 non-overlapping random fields of view per replicate (right panel). *n* = 4 experimental replicates. Data shown as the mean +/− s.e.m. *P*

values were determined by Student's two-tailed *t*-test. Scale bar, 20 µm. **c** Representative image of KLF4-BRG1 PLA in healthy rat lung tissue. The original PLA protocol was modified with longer incubation times to allow the reagents to fully penetrate the 350 µM thick sections. Note the interaction of KLF4 with BRG1 at straight sites of the vasculature that are exposed to LSS (upper left insert), while sites at bifurcations which are exposed to disturbed shear stress (DSS) do not show the KLF4-BRG1 interaction (bottom right insert). Bar graphs show the average number of foci per nucleus quantified in regions of DSS or LSS at 6 random bifurcations. KLF4-BRG1 interaction (magenta); vWF (gray, pseudo-color); αSMA (green). Nuclei were stained with DAPI, (blue). Scale bar, 20 and 10 µm in the higher magnifications. Data shown as the mean +/− s.e.m. *P* value was determined by Student's two-tailed *t*-test. Source data are provided as a Source Data file.

accessibility and facilitate transcriptional activation, including the lysine demethylase KDM2A and Bromodomain Containing 4 (BRD4), as well as remodelers that decrease accessibility resulting in transcriptional repression, such as histone deacetylase HDAC2 and DNA methyltransferases DNMT1 and DNMT3A (Fig. 3a).

To confirm the interaction between KLF4 and the SWI/SNF complex in cells and tissue, we performed in situ proximity ligation assays (PLA) for KLF4 and either BRG1 or SMARCC2, which requires the epitopes of both proteins to be within 40 nm of each other to be detected. Indeed, in PAEC exposed to LSS, we observed the interaction between KLF4 and both SWI/SNF components (Fig. 3b). To determine if this interaction also occurs in the intact vessel wall, we modified the PLA protocol to allow us to study the interaction between KLF4 and the SWI/SNF complex in the rat pulmonary vasculature. Since SMARCC2 is a core subunit of the SWI/SNF chromatin remodeling complex that co-localizes with BRG1, we focused these studies on the interaction

between KLF4 and BRG1. Using deep tissue imaging we studied regions with bifurcations to allow us to compare straight parts of the vessel exposed to LSS, with branching points that are exposed to disturbed shear stress (Supplementary Fig. 9). The KLF4-BRG1 interaction was prominent at sites of LSS and much less apparent at regions with disturbed flow (Fig. 3c).

KLF4 and BRG1 co-occupied regions show an enhancer chromatin signature

To study the genome wide chromatin accessibility changes co-regulated by KLF4 and BRG1, we intersected KLF4 and BRG1 peaks from the caMEK5 ChIP-Seq data with the ATAC-Seq data of PAEC exposed to LSS. Of the 8,404 regions that were enriched for both KLF4 and BRG1, 2,955 were found at DAR that open with LSS, representing 62.9% of all LSS DAR (Fig. 4a). In contrast, KLF4-BRG1 co-occupancy was only found at 4.2% of accessible regions that were not differentially
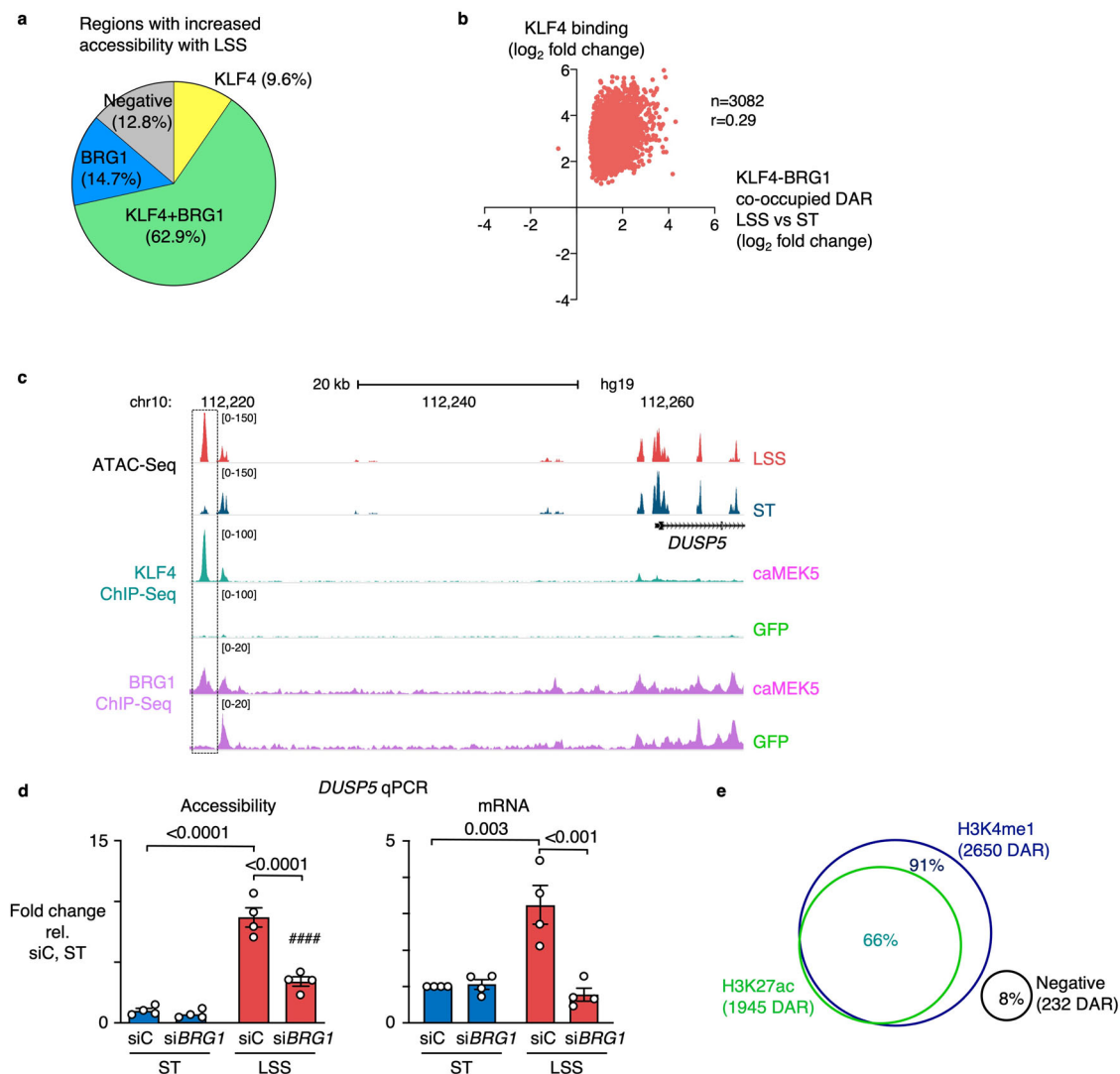

Fig. 4 | KLF4 and BRG1 co-occupy regions with increased accessibility under LSS, most of which are distal enhancers. a Pie chart depicting the intersection of regions with increased accessibility under LSS by ATAC-Seq, with KLF4 and BRG1 ChIP-Seq data from PAEC transduced with caMEK5. Percentages indicate the fraction of DAR with increased accessibility under LSS vs ST that are differentially enriched for KLF4 and/or BRG1. **b** Scatterplot showing the correlation between KLF4 binding and accessibility changes at LSS vs ST DAR co-occupied by KLF4-BRG1. Indicated values were calculated by a two-tailed Pearson R test, with $P < 0.0001$. **c** ATAC-Seq and KLF4 and BRG1 ChIP-Seq tracks showing enrichment

for both factors at the DAR 39 Kb upstream of *DUSP5*. **d** PAEC were treated with siRNA targeting BRG1 (siBRG1) or with non-targeting controls (siC) prior to exposure to 15 dyn/cm^2 of LSS or ST conditions for 24 h. Bar graphs indicate accessibility of the DAR 39 Kb upstream of *DUSP5*, and *DUSP5* gene expression, both assessed by qPCR. **e** Venn diagram showing the percentage of KLF4-BRG1 co-occupied DAR with increased accessibility under LSS, that are enriched for H3K4me1 and H3K27ac. $n = 2$ experimental replicates for **a–c, e**, and $n = 4$ experimental replicates for d. Data are shown as the mean ± s.e.m. P values were determined by Student's two-tailed t-test. Source data are provided as a Source Data file.

accessible with LSS (Supplementary Fig. 10a) and was only present in a small subset of DAR (2.1%) that lose accessibility under LSS (Supplementary Fig. 10b). An increase in KLF4 binding at KLF4-BRG1 co-occupied DAR was associated with increased accessibility (Fig. 4b).

Increased BRG1 peaks were found at 77.6% of DAR with increased accessibility under LSS (Fig. 4a), as well as at 53.7% of DAR that have increased accessibility under ST conditions (Supplementary Fig. 10b), but only in 13.5% of regions that were not differentially accessible (Supplementary Fig. 10a), demonstrating that BRG1 binding coincides with increased chromatin accessibility even under ST conditions. In addition, when plotting changes in BRG1 binding at LSS vs ST DAR, we found that increased BRG1 binding correlates with an increase in accessibility, and a decrease in BRG1 with loss of accessibility ($r = 0.89$, $p < 0.0001$) (Supplementary Fig. 10c).

An example of a KLF4-BRG1 co-occupied site is the DAR 39 Kb upstream of *DUSP5* that we had previously identified by ATAC-Seq (Fig. 4c and Supplementary Fig. 11a). We also studied KLF4-BRG1 binding at DAR located at the *COL3A1*, *ITGB4*, *ITGA6*, *DLL1*, and *HYAL1* loci that were illustrated before (Supplementary Fig. 8). In all cases, we found enrichment for KLF4, generally coinciding with increased BRG1 occupancy (Supplementary Fig. 11b–f). In one of the DAR upstream of *ITGB4*, BRG1 occupancy and chromatin accessibility were also high under ST conditions, suggesting that this site is regulated by other factors under ST conditions. (Supplementary Fig. 11c).

To confirm that BRG1 is required for the chromatin accessibility changes, we transfected PAEC with siRNA targeting BRG1 prior to exposure to LSS (Supplementary Fig. 10d). Indeed, loss of BRG1 decreased chromatin accessibility of the DAR upstream of *DUSP5* as assessed by ATAC-qPCR, coinciding with reduced *DUSP5* mRNA transcript levels (Fig. 4d).

To further characterize KLF4-BRG1 co-occupied regions, we performed ChIP-Seq for the H3K4me1 enhancer mark, as well as for H3K27ac which is typically present at active enhancers and promoter regions. The majority of KLF4-BRG1 co-occupied regions were enhancers marked by H3K4me1 (91%, Fig. 4e) two-thirds of which were also marked by H3K27ac (66%, Fig. 4e).

KLF4 regulates gene expression by binding at enhancer loops

Thus far, we have related chromatin accessibility changes to gene expression based on the nearest gene. However, we found a direct relationship in only a subset of DEG, possibly because several enhancers target a particular gene, or because enhancer loops can skip promoters of proximal genes to target a more distal gene. We, therefore, applied two complementary strategies to map enhancer-promoter regulation: H3K27ac HiC Chromatin Immunoprecipitation (HiChIP), which measures the frequencies of 3D contacts between enhancers and promoters[19,20], and the Activity-By-Contact (ABC) algorithm, that predicts enhancer-promoter interactions based on ATAC-Seq and H3K27ac ChIP-Seq data[21].

Significant chromatin loops identified by HiChIP were determined using FitHiChIP[30]. At a one Kb resolution, we identified 4698 enhancer-promoter (EP) loops, of which 1,299 were differential between LSS and ST conditions. We then integrated these data with KLF4 ChIP-Seq to study KLF4 binding at enhancer anchor and found differential KLF4 binding at 856 enhancer anchors that regulate 325 DEG (Fig. 5a). To determine whether KLF is required to form these EP loops, we performed H3K27ac HiChIP in PAEC treated with siRNA targeting KLF2/4 prior to exposure to LSS. More than a third of the enhancer anchors were lost with KLF siRNA. The enhancer anchors that were lost targeted more than half of the DEG that are regulated by EP loops in wildtype PAEC exposed to LSS (Fig. 5b).
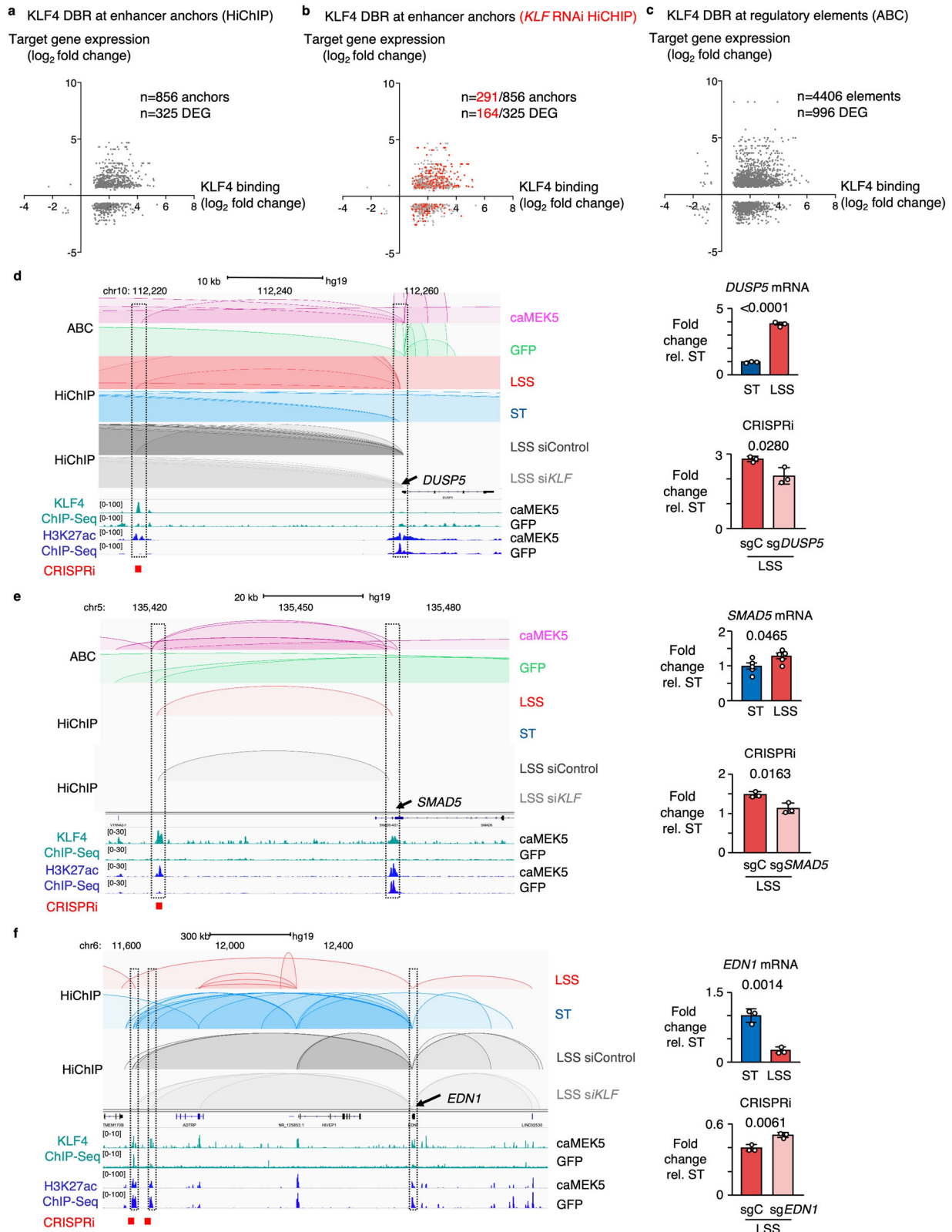
The ABC algorithm predicts which distal elements regulate which genes, considering elements located at both shorter (<10 Kb) and longer (>10 Kb) ranges[21]. The algorithm scores elements based on chromatin accessibility determined by ATAC-Seq and the strength of

the H3K27ac enhancer signal at those sites and has been validated by perturbing thousands of putative enhancers using CRISPR interference (CRISPRi)[21]. The algorithm predicted 996/1,383 DEG under LSS to be regulated by enhancer elements that were occupied by KLF4 (Fig. 5c). ABC confirmed most of the enhancer loops that were identified by HiChIP, for example, the DAR that was observed near *DUSP5* (Fig. 5d and Supplementary Figs. 11a, 12), as well as one targeting *SMAD5*, a transcriptional effector of BMPR2 signaling (Fig. 5e and Supplementary Fig. 13). Both loops were lost when PAEC were treated with KLF RNAi prior to exposure to LSS (Fig. 5d, e).

KLF4 also occupied enhancer anchors of loops that were lost with LSS, associated with a reduction in H3K27ac levels at those sites and a decrease in target gene expression. These include two enhancer anchors of EP loops that we identified to target endothelin-1 (*EDN1*), a potent vasoconstrictor that is elevated in patients with PAH, and a major therapeutic target[31,32]. In caMEK5-transduced cells, there was increased binding of KLF4 at these sites with a concomitant decrease in H3K27ac levels (Fig. 5f and Supplementary Fig 14). When we performed H3K27ac HiChIP in PAEC treated with KLF siRNA prior to exposure to LSS, both loops remained present (Fig. 5f). Based on our AP-MS data (Fig. 3a), we speculate that under this condition, KLF4 might interact with HDAC2 to inactivate the enhancer, resulting in decreased *EDN1* mRNA levels (Fig. 5f). In smooth muscle cells, the interaction between KLF4 and HDAC2 promotes transcriptional silencing of SM22α[33].

We then went on to functionally validate these enhancers using CRISPRi. We transduced PAEC with a lentiviral vector encoding a doxycycline-inducible mutant of a catalytically dead Cas9 fused to the bipartite repressor domain MeCP2-KRAB[34]. We designed synthetic guide RNAs (sgRNA) to target the predicted KLF binding motifs in the candidate enhancer regions, and analyzed target gene expression by RT-qPCR following 24 h of exposure to LSS. Disruption of the *DUSP5* and *SMAD5* enhancers by CRISPRi resulted in decreased expression of their target genes (Fig. 5d, e), illustrating that they are *bonafide* enhancers. CRISPRi-mediated disruption of those same sites under ST conditions had no effect on target gene expression, indicating that these regulatory sites are specifically activated under LSS (Supplementary Fig. 15). CRISPRi-mediated inactivation of the *EDN1* enhancer sites resulted in an increase in *EDN1* gene expression under LSS, confirming that these enhancer elements are repressed under LSS (Fig. 5f and Supplementary Fig. 15).

The ABC algorithm predicted many shorter-range EP interactions that were not discovered by HiChIP, including two enhancers for the canonical Notch target gene *HES2*, that has previously been described to be regulated by shear stress[35] (Supplementary Fig. 16). One of these enhancers was identified based on increased chromatin accessibility, despite low H3K27ac expression levels at that site. HiChIP also identified long-range EP loops, often spanning multiple genes, which were not predicted by the ABC algorithm, likely because the distance of an enhancer element to its target gene is a component of the algorithm, favoring shorter range interactions as enhancers are more likely to affect proximal genes. An example is an enhancer loop that spans several genes to target the promoter region of *BMPR2*. Mutations in the coding and proximal regulatory regions of this gene have been identified in patients with PAH[16,17], but there might also be mutations in this distal enhancer that have not previously been linked to *BMPR2*. We identified a KLF4 bound EP loop with increased H3K27ac levels at the enhancer anchor located 1.3 Mb downstream of the *BMPR2* transcription start site, associated with a 2-fold increase in *BMPR2* mRNA levels under LSS (Supplementary Fig. 17). When attempting to silence the enhancer using CRISPRi, we did not observe a significant decrease in *BMPR2* mRNA expression, possibly because the proximal enhancers have more pronounced affects or they act in concert with each other, or because the gRNAs did not effectively target the enhancer region.

a KLF4 DBR at enhancer anchors (HiChIP)

Target gene expression (log$_2$ fold change)

n=856 anchors
n=325 DEG

KLF4 binding (log$_2$ fold change)

b KLF4 DBR at enhancer anchors (*KLF* RNAi HiChIP)

Target gene expression (log$_2$ fold change)

n=291/856 anchors
n=164/325 DEG

KLF4 binding (log$_2$ fold change)

c KLF4 DBR at regulatory elements (ABC)

Target gene expression (log$_2$ fold change)

n=4406 elements
n=996 DEG

KLF4 binding (log$_2$ fold change)

Non-coding variants at KLF4 bound enhancers are associated with vascular disease

More than 90% of single nucleotide polymorphisms (SNPs) identified in whole genome-wide association studies occur in non-coding regions[36]. Since our data indicate that KLF4 regulates endothelial gene expression through enhancer activation, we explored whether genetic variants occur in KLF4 bound distal enhancers, as this may

explain how SNPs in non-coding regions might predispose to vascular disease. We intersected KLF4 bound enhancer elements identified by ABC with variants associated with blood pressure traits from a recent genetic association study that included over 1 million people[37]. We found 22 SNPs associated with hypertension in enhancer elements predicted to target 35 genes (Supplementary Fig. 18a). This included rs933795, which is also associated with coronary artery disease[38,39].

Fig. 5 | KLF4 modulates gene expression through changes in the enhancer landscape. a Scatterplot showing the relation between differential KLF4 binding at enhancer anchors identified by HiChIP, with target gene expression, in PAEC exposed to 15 dyn/cm² of LSS vs ST conditions for 24 h. **b** Scatterplot showing the loss of enhancer anchors identified by HiChIP upon KLF siRNA (marked in red), and their impact on target gene expression. HiChIP enhancer anchors were derived from PAEC treated with KLF RNAi for 48 h prior to exposure to 15 dyn/cm² of LSS vs ST conditions for an additional 24 h. **c** Scatterplot showing the relation between KLF4 binding at enhancer anchors identified by ABC, with target gene expression. $n = 2$ experimental replicates. **d** ABC, HiChIP and ChIP-Seq tracks illustrating a KLF4 bound enhancer loop targeting *DUSP5*, which is lost with KLF siRNA (left panel). *DUSP5* mRNA was determined by RT-qPCR in PAEC exposed to 15 dyn/cm² of LSS vs ST conditions for 24 h (top right panel). Silencing the enhancer by CRISPRi decreased *DUSP5* mRNA levels (bottom right panel). **e** ABC, HiChIP, and ChIP-Seq

tracks illustrating an enhancer loop targeting *SMAD5*, which was lost with KLF RNAi (left panel). *SMAD5* mRNA was determined by RT-qPCR in PAEC exposed to 15 dyn/ cm² of LSS vs ST conditions for 24 h, and shown normalized to ST expression levels (top right panel). Silencing the enhancer by CRISPRi, decreased *SMAD5* mRNA levels (bottom right panel). **f** ABC, HiChIP and ChIP-Seq tracks illustrating enhancer loops that target *EDN1* under ST conditions, which are lost with LSS but are present with KLF siRNA (left panel). *EDN1* mRNA was determined by RT-qPCR in PAEC exposed to 15 dyn/cm² of LSS vs ST conditions for 24 h (top right panel). Silencing the enhancer increased *EDN1* mRNA levels (bottom right panel). For **a** and **b**, $N = 2$ experimental replicates for KLF4 ChIP-Seq; $n = 3$ experimental replicates for HiChIP. For **d**–**f**, data are shown as the mean +/− s.e.m. For mRNA expression $n = 5$ experimental replicates; for CRISPRi experiments $n = 3$ replicates. P values were determined by Student's two-tailed t-test. Source data are provided as a Source Data file.

This SNP is predicted to target an enhancer for junctional cadherin 5 associated protein (*JACD*), which was found to regulate the response of endothelial cells to shear stress[40].

Another example is rs3918226, a variant located in the promoter of *NOS3*, which is associated with an increased risk for systemic hypertension[41]. This variant is thought to negatively affect transcription of the *NOS3* gene, resulting in decreased NO bioavailability[40], however healthy subjects with this variant do not have altered plasma nitrite levels, suggesting a NOS3 independent effect[42]. Interestingly, it is located at a KLF4 bound enhancer that under LSS, targets *AGAP3*, a GTPase-activating protein that interacts with myosin phosphatase which regulates endothelial permeability[43] (Supplementary Fig. 18b). The polymorphism may result in increased permeability, facilitating pro-inflammatory activation that could lead to vascular stiffening. While it is probable that this variant impairs *NOS3* expression by interfering with *NOS3* promotor activation, these data indicate that dysregulation of *AGAP3* may also contribute to the increased risk for systemic hypertension.

Discussion

KLF2 and KLF4 are well-recognized LSS-induced transcription factors that control endothelial homeostatic gene regulation[9–13]. Our studies indicate that KLF4, beyond its previously established role as a transcriptional activator of vasculoprotective gene expression, can act as a chromatin organizer by recruiting the SWI/SNF chromatin remodeling complex to alter chromatin accessibility and regulate the endothelial enhancer landscape (Fig. 6).

Shear forces exerted by blood flow are sensed by endothelial cells and converted to protective or vulnerable gene expression profiles through mechanotransduction. Identification of mechanosensing complexes and their downstream signaling pathways has been the subject of extensive investigation and has greatly improved our understanding of how spatiotemporal changes in hemodynamics affect endothelial function and vascular homeostasis[6–8]. More recently, the epigenetic regulation of shear stress-mediated gene expression has gained increasing attention. Illi et al. were the first to report the importance of H3 and H4 histone modifications in the regulation of LSS-induced gene expression[44]. Many studies followed that investigated the role of histone acetyltransferases and deacetylases, as well as the histone methyltransferase EZH2, in mediating shear stress-induced gene expression changes both in vitro and in vivo[45–49]. Other studies have addressed the role of DNA methylation and the contribution of DNA methyltransferases (DNMT) in the regulation of gene expression by shear stress[50–52], including the identification of DNMT3A-dependent KLF4 promoter hypermethylation by disturbed flow[52].

He and colleagues recently demonstrated that KLF4 regulates Inositol 1,4,5-trisphosphate receptor type 3 (*IPTR3*) expression by increasing chromatin accessibility and H3K27 acetylation at the *ITPR3* promoter region[53]. In addition, many microRNAs are shear stress-regulated[54], perhaps most notably miR-92a, that targets KLF2 and KLF4

under conditions of disturbed flow[55,56]. More recently, long non-coding RNAs (lncRNAs) have been studied as epigenetic regulators of shear stress-induced gene expression, leading to the discovery of spliced-transcript endothelial-enriched lncRNA (STEEL)[57] and a lncRNA that enhances *NOS3* expression (LEENE)[58].

Yet despite these advances, no studies have comprehensively mapped the endothelial regulatory landscape under physiologic LSS. While transcription factor binding to gene promoters is sufficient to drive basal levels of transcription[59], activation of enhancers is required for full transcriptional activity[60] and to ensure phenotypic robustness[61]. In cultured cells, persistent changes in the epigenome may be particularly revealing of mechanisms that converge to cause disease[62].

To investigate LSS-induced changes to the chromatin landscape, we performed ATAC-Seq on PAEC that were exposed to physiologic LSS of 15 dyn/cm² for 24 h. Only a small subset of DAR were located in gene promoter regions, the majority being putative regulatory elements in introns or intergenic sites. For KLF gain-of-function studies, and to have sufficient cell numbers for ChIP-Seq analyses, we used PAEC that were transduced with a vector encoding a constitutively active mutant of MEK5, resulting in activation of ERK5 and induction of KLF2 and KLF4 via MEF2[26,27]. KLF2 and KLF4 expression levels were induced to physiologic levels, i.e., similar to those observed in wildtype cells exposed to LSS. Although we cannot rule out KLF-independent effects resulting from ERK5 activation, such as through induction of NF-E2-related Factor 2 (Nrf2)[63] or direct effects of MEF2 activation, motif enrichment analyses of wildtype cells exposed to LSS revealed that MEF2 motifs were not in the top 20 most enriched motifs, with 17% of DAR having predicted MEF2 binding sites. We did not find enrichment for Nrf2 binding sites in DAR under LSS, corroborating the role of KLF in mediating the changes in accessibility. We focused our analyses on KLF4-occupied DAR that were common to wildtype PAEC exposed to LSS and those transduced with caMEK5. While recent technological advances, e.g., CUT&RUN[64], allow for lower cell inputs to study protein-chromatin interactions based on histone modifications, these strategies are generally less comprehensive when studying transcription factor binding.

ChIP-Seq analyses of H3K4me1 and H3K27ac confirmed that most of these DAR have a chromatin signature typical of enhancers. Motif enrichment analysis of DAR with increased accessibility under LSS pinpointed the KLF transcription factor family as potential regulators of the accessibility changes. KLF4, in particular, has gained a lot of interest, being one of the four original reprogramming factors used by Takahashi and Yamanaka to create induced pluripotent stem cells (iPSC)[65]. This finding initiated further investigations into its role as a pioneer factor. Upon initial engagement of closed chromatin, pioneer factors recruit chromatin remodelers to allow stabilization of accessible chromatin, enabling other transcription factors to bind alongside them and recruit transcriptional machinery[66]. In vitro, purified KLF4 binds nucleosomes, and in vivo KLF4 preferentially targets closed
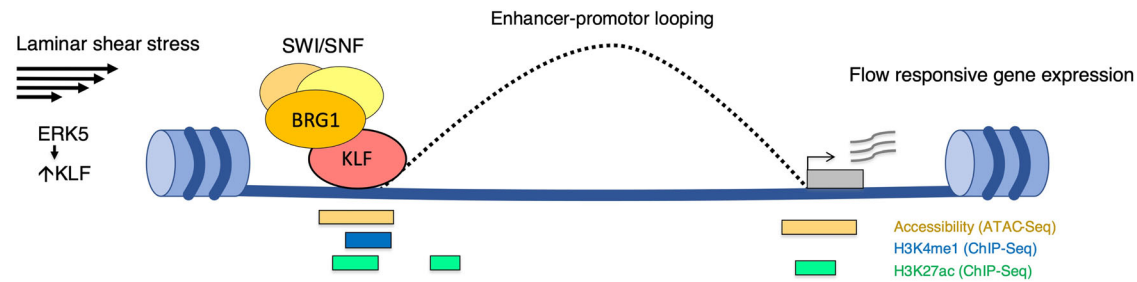
Fig. 6 | Model illustrating the role of KLF in regulating the endothelial enhancer landscape under LSS. Laminar shear stress induces KLF, which interacts with the SWI-SNF chromatin remodeling complex to increase chromatin accessibility at gene regulatory regions and promote enhancer-promotor looping to LSS-responsive genes to increase gene expression.

chromatin enriched for condensed nucleosomes[67]. Our KLF4 ChIP-Seq data corroborate these findings, showing KLF4 binding at 72.5% of regions that have increased accessibility versus 19.2% of regions that are constitutively accessible.

In the induction of pluripotency, KLF4 predominantly binds distal enhancers of genes that promote reprogramming, unless it partners with c-myc, in which case it tends to bind promoter regions[68]. This was confirmed in our data, in which 70.3% of KLF4 binding occurs outside of gene promoters that are within 3 Kb of transcription start sites. It would be interesting to identify which transcriptional co-factors guide KLF4 to either distal enhancers or promoter regions. Given the enrichment for the ETS motifs in DAR, and the well-established roles for ETS factors in regulation of endothelial gene expression[23,24], we speculate that distinct ETS family members may play important roles in guiding these processes. At sites that were accessible under both LSS and ST conditions, a change in chromatin accessibility may not be a prerequisite for KLF to increase enhancer activity. Conversely, while the majority of DAR depend on KLF to increase accessibility, additional factors may be required for enhancer activation.

Besides DNA methylation and histone modifications, ATP-dependent chromatin remodeling processes such as the mammalian SWI/SNF complex, are important regulators of chromatin accessibility by disrupting histone-DNA contacts[69]. The SWI/SNF remodeling complex can assist transcriptional activators to access closed chromatin[70–72] or facilitate subsequent transcriptional activation[73]. For example, in mouse embryonic stem cell differentiation, the pioneer factor Forkhead Box A2 (FOXA2) binds regions of closed chromatin and recruits SWI/SNF to regulate nucleosome depletion and to promote endodermal differentiation[74]. More recently, BRG1, one of two mutually exclusive ATPases that functions as the catalytic subunit of the SWI-SNF complex[75], was related to the reprogramming of iPSCs by increasing the accessibility of pluripotency enhancers[76]. Alver and colleagues described SWI/SNF as required for maintenance of lineage-specific enhancers[77].

While BRG1 co-localizes with pluripotency factors OCT4, SOX2, and NANOG in embryonic stem cells[78], to our knowledge there have been no prior reports of KLF4 and SWI/SNF co-localization or interaction, other than a high throughput lentiviral proteomics study that identified an interaction between KLF4 and Brahma (BRM) which is closely related to BRG1, but mutually exclusive[79]. Because BRG1 is not regulated by shear stress, we speculate that under conditions of disturbed shear stress BRG1 might interact with AP1 family members, as we found enrichment for these motifs in DAR that are losing accessibility with LSS.

Since physical distance is an important indicator of the probability that a regulatory element targets a certain gene, we initially related DAR to their nearest gene. While accessibility changes generally correlated with gene expression changes, this could only explain a subset of gene regulation. The seminal work by Dekker and colleagues, who first described chromosome confirmation capture (3C)[80], initiated

further development of 3C-derived methods, including landmark studies applying Hi-C[81,82]. This greatly improved our understanding of the 3D genome and helped explain how regulatory elements that are megabases away from their target promoter region in the linear genome are in fact in close physical proximity. To map the endothelial enhancer landscape and study the contribution of KLF4 and BRG1 in regulating enhancer activity and target gene expression, we applied two distinct but complementary strategies to study enhancer-promoter (EP) looping, i.e., H3K27ac HiChIP[19,20] and the Activity-by-Contact model (ABC)[21]. The experimental H3K27ac HiChIP approach detects the frequency of 3D contacts and identified many long-range EP loops that often span genomic regions containing multiple genes. The computational ABC algorithm, that was extensively validated by thousands of CRISPRi perturbations[21], confirmed most of the EP loops that were identified by HiChIP and discovered many additional EP loops. ABC predicted more than 70% of differentially expressed genes to be regulated by KLF4-bound enhancers, reinforcing the pivotal role of KLF4 as the mediator of the vasculoprotective effect of LSS. The importance of KLF4 in regulating the endothelial enhancer landscape is further supported by a recent study that uncovered a critical role for KLF4 in organizing the pluripotency-associated enhancer network[83]. Here we show, using KLF loss-of-function by siRNA, that a large subset of EP loops is indeed KLF dependent. We applied CRISPRi to functionally validate candidate enhancers that we found are regulated by LSS, and are particularly relevant to pulmonary vascular homeostasis and PAH, i.e., *BMPR2*, *SMAD5*, and *EDN1*. We observed KLF4 binding at enhancers of other genes associated with PAH, such as *ACVRL1*, *CAV1*, *ENG*, *SMAD9*, and *SOX17*, but their expression levels did not significantly change under LSS. Additional genetic and/or environmental factors can contribute to the altered regulation of these genes, and more extensive whole genome sequencing studies may reveal mutations in binding sites for other transcription factors that might act in concert with KLF.

In most cases, KLF4 binding at enhancers resulted in increased target gene expression. However, in some, such as the EP loops targeting endothelin-1, KLF4 binding resulted in reduced H3K27ac and target gene expression, possibly by recruiting histone deacetylases such as HDAC2 that we identified to interact with KLF4 by AP-MS, and that others have shown to interact with KLF4 in smooth muscle cells[32]. These opposing changes in gene regulation reflect the diversity of remodelers that we identified as KLF4 interactors and warrant further study to understand how KLF4 binding results in different outcomes at different sites.

Our findings can be leveraged to better relate genetic variants in non-coding regions identified by genome-wide association studies (GWAS) to protective or pathogenic gene expression. An example that we described is a variant in the *NOS3* promoter that may target *AGAP3*. Most single nucleotide polymorphisms (SNPs) identified by GWAS occur in non-coding regions[35], and individually often contribute small or indirect effects to complex traits. Knowing the endothelial enhancer

landscape under physiologic LSS will facilitate linking variants identified by GWAS to specific genes, and to uncover other genes that have not been related to cardiovascular disease before, especially in rare conditions such as PAH. Future studies applying CRISPRi or base editing approaches to target SNPs in candidate enhancers, or broader approaches using pooled CRISPR screens combined with single cell RNA-Seq, such as Perturb-Seq[84], are needed to validate the impact of these non-coding variants on the genes that they regulate, and to determine how this may contribute to the prevention or progression of disease.

Methods

Ethical approval

Procedures were compliant with all ethical regulations regarding animal research. Care and housing of the rats was in accordance with the guidelines from the Stanford University Administrative Panel on Laboratory Animal Care and approved under APLAC protocol 31608. Human cells provided by the PHBI Initiative were obtained under the PHBI network IRB protocol, with informed consent and IRB approvals at the transplant procurement sites. The cell lines used were coded with no identifying information and therefore considered non-human subject research for the purposes of this study. Cells purchased from PromoCell were derived from tissues of donors who have signed an informed consent form. In both cases, the informed consent outlines in detail the purpose of the donation and the procedure for processing the tissue.

Cell culture studies

Primary human pulmonary artery endothelial cells (PAEC) were either commercially obtained (PromoCell) or harvested from unused donor control lungs obtained though the Pulmonary Hypertension Breakthrough Initiative (PHBI) funded by NIH (R24 HL123767) and the Cardiovascular Medical Research and Education Fund (CMREF; UL 1RR024986). PAEC were grown in commercial EC media containing 5% FBS (Sciencell) in a 5% CO_2 air atmosphere and used at passages 3–7. Cells were routinely tested for mycoplasma contamination. For shear stress experiments, PAEC were seeded in flow chamber slides (μ-Slide I 0.4 mm ibiTreat; Ibidi) and grown to confluence before exposure to 15 dyn/cm² of unidirectional uniform laminar shear stress (LSS) for 24 h. LSS was generated using the Ibidi Perfusion System (Ibidi). Static controls were performed simultaneously with the shear stress experiments, cultured on standard tissue culture treated plates or dishes using the same EC media (Sciencell), to avoid nutrient deprivation that can occur in flow chamber slides that are not perfused.

RNAi

PAEC were transfected with ON-TARGETplus SMARTpool RNAi targeting *KLF2* (L-006928-00-0005, Dharmacon), *KLF4* (L-005089-00-0005, Dharmacon) and *DUSP5* (L-003566-00-0005, Dharmacon) or ON-TARGETplus non-targeting pool (D-001810-10-05, Dharmacon) as siControl. Transfection was performed using Lipofectamine RNAiMAX in Opti-MEM 1 reduced serum medium (ThermoFisher) for 7 h, after which media were changed to regular ECM (Sciencell). 48 h after the start of transfection transfected PAEC were exposed to LSS or ST conditions for 24 h.

Plasmids

PAEC were transduced with adenoviral constructs encoding a constitutive active mutant of dual specificity mitogen-activated protein kinase 5 (caMEK5) (#000101 A, Applied Biological Materials Inc); Flag-tagged KLF4 (#VH829440, Vigene Biosciences) or GFP control (AVP004, GenTarget Inc) for 12 h after which cells were allowed to recover for 90 h before being harvested for subsequent experiments. For CRISPRi studies, PAEC were transduced with a lentiviral vector encoding a doxycylin-inducible mutant of a catalytically dead Cas9 fused to the bipartite repressor domain MeCP2-KRAB (Addgene Plasmid #122205) for 12 h and allowed to recover for 90 h followed by selection with blasticidin (10 μg/ml).

ATAC-seq sample preparation and data analysis

ATAC-seq was performed as described in Buenrostro et al.[85]. Briefly, endothelial cells were trypsinized to create a single-cell suspension. After counting, nuclei were isolated from 100,000 cells and sequencing adapters were transposed for 30 min at 37 °C using 5 μl of TDE1 (Nextera Tn5 transposase, Illumina). After PCR and gel purification, libraries were subjected to 2 × 151 paired end sequencing on the Illumina HiSeq 4000 to obtain an average of approximately 50 million uniquely mapped reads per sample (Stanford Center for Genomics and Personalized Medicine, supported by NIH grant S10OD020141). The resulting data were processed using the Kundaje Lab ATAC-seq processing pipeline (https://github.com/kundajelab/atac_dnase_pipelines). Briefly, this pipeline takes FASTQ files as input, and outputs peak calls (accessible regions, AR). Alignments to AR were counted using DiffBind v2.4.8 (https://rdrr.io/bioc/DiffBind/) to produce a count matrix. DAR were detected using DESeq2 (https://bioconductor.org/packages/release/bioc/html/DESeq2.html) with a P-value cutoff of <0.1. The HOMER (http://homer.salk.edu/homer/) function findMotifsGenome was used with default parameters to search for motif enrichment in the full accessible regions.

RNA-seq sample preparation and data analysis

RNA was extracted using the RNeasy Mini Kit (#74136, Qiagen). Libraries were prepared using TruSeq Stranded Total RNA Library Prep Kit with Ribo-Zero Gold (Illumina) for experiments with PAEC exposed to LSS vs ST, caMEK5 vs GFP, and *KLF2/4* RNAi studies, and using QuantSeq 3′ mRNA-Seq Library Prep Kit REV for Illumina (#016.96, Lexogen) for the *DUSP5* RNAi study. Sequencing on the Illumina HiSeq 4000 yielded an average of approximately 8 million uniquely mapped reads for total RNA-Seq, and 7 million uniquely mapped reads per sample for mRNA-Seq (Supplementary Table 1; Stanford Center for Genomics and Personalized Medicine, supported by NIH grant S10OD020141). The resulting data were aligned to the human genome (GRCh37.p13) by STAR v.2.5.4b (https://github.com/alexdobin/STAR). The aligned transcripts were quantitated based on features in the GENCODE annotation database (GRCh37, version 19) by RSEM v. 1.3.1 (http://deweylab.biostat.wisc.edu/rsem/). Differentially expressed genes were detected using DESeq2 v. 1.20.0 (https://bioconductor.org/packages/release/bioc/html/DESeq2.html) with a P-value cutoff of <0.1. Functional enrichment for the differentially expressed genes was performed using Metascape.

ChIP-seq sample preparation and data analysis

For KLF4, H3K4me1, and H3K27ac ChIP-Seq, cells were trypsinized and cross-linked with 1% formaldehyde (EMD Millipore) for 10 min at RT. To quench the formaldehyde, 2 M glycine (ThermoFisher Scientific) was added and incubated for 5 min at room temperature. For BRG1 ChIP-Seq, cells were first cross-linked using 2 mM of DSG (Pierce) for 45 min at RT, washed with PBS, and then cross-linked with 1% formaldehyde as described above. Cells were washed with ice cold PBS twice, snap-frozen and stored at −80 °C. For ChIP-DNA preparation, cells were thawed by adding PBS and incubated at 4 °C with rotation. Cells were treated with hypotonic buffer (20 mM HEPES pH 7.9, 10 mM KCl, 1 mM EDTA pH 8.0, 10% glycerol) for 10 min on ice in the presence of protease inhibitors (G6521, Promega), then were homogenized using a glass homogenizer. Nuclear pellets were resuspended in RIPA buffer (Millipore) and incubated for 30 min on ice. Chromatin corresponding to 20 million cells for transcription factors, or 5 million cells for histone modifications was sheared with SFX250 Sonifier (Branson) and immunoprecipitated with antibodies targeting H3K27ac (#8173, Cell signaling Technology), H3K4me1 (#5326, Cell Signaling Technology),

KLF4 (sc20691, Santa Cruz Biotechnology) and BRG1 (A303-877A, Bethyl Laboratories); 5 µg for each condition, at 4 °C overnight on a nutator. For the input sample, 100 µl of sheared nuclear lysate was removed and stored overnight at 4 °C. The next day, protein A/G agarose beads (Millipore) were added to the chromatin-antibody complex and incubated for one hour at 4 °C on a nutator, after which the beads were eluted with SDS buffer (Santa Cruz Biotechnology) and incubated at 65 °C for 10 min. Supernatant containing ChIP-DNA was reverse crosslinked by incubating overnight at 65 °C. On the third day, ChIP-DNA was treated with RNase A (Qiagen) and proteinase K (ThermoFisher Scientific) and then purified. The ChIP-DNA samples were end repaired using End-It DNA End Repair Kit (Lucigen) and A-tailed using Klenow Fragment and dATP (New England Biolabs). Illumina TruSeq adapters (Illumina) were ligated using LigaFast (#M8221, Promega) and size-selected by gel extraction before PCR amplification. The purified libraries were subjected to 2 × 151 paired end sequencing on the Illumina HiSeq 4000 to obtain an average of approximately 37 million uniquely mapped reads for each sample (Supplementary Table 1; Stanford Center for Genomics and Personalized Medicine, supported by NIH grant S10OD020141). The resulting data were processed using the Kundaje Lab ChIP-seq processing pipeline (https://github.com/kundajelab/chipseq_pipeline). Briefly, this pipeline takes FASTQ files as input and outputs peak calls (bound regions; BR). Alignments to BR were counted using DiffBind 2.4.8 (https://rdrr.io/bioc/DiffBind/) to produce a count matrix. Differentially bound regions (DBR) were detected using DESeq2 (https://bioconductor.org/packages/release/bioc/html/DESeq2.html) with a *P*-value cutoff of <0.1. Data visualization was performed using the Integrative Genomics Viewer (http://www.broadinstitute.org/igv).

Immunofluorescence

PAEC were cultured on flow slides (µ-Slide I 0.4 mm ibiTreat; Ibidi), washed with PBS, and fixed with ice-cold methanol at −20 °C for 30 min. Methanol was aspirated and the slides were rehydrated with PBS at room temperature for 10 min. After washing with PBS, slides were blocked with 5% normal donkey serum and 2% BSA (Sigma Aldrich) in PBS at room temperature for 1 h. Incubation with primary antibodies targeting KLF4 (1:100, sc20691, Santa Cruz Biotechnology), ATF2 (1:100 sc-242, Santa Cruz Biotechnology) and ETS1 (1:100, sc55581, Santa Cruz Biotechnology) were carried out in the blocking buffer at 4 °C overnight. Secondary antibody incubations were performed using 1:600 dilutions of A-21206 (for KLF4); A-21203 (for ATF2) and A-31571 (for ETS1), all from ThermoFisher Scientific, in the blocking buffer at room temperature for 1 h. Slides were mounted with DAPI Fluoromount-G (DAPI, 4,6-diamidino-2-phenylindole) (SouthernBiotech). Stained slides were imaged using Leica Application Suite X software on a Leica Sp8 (Leica). Quantification of the nuclear fluorescence intensities was performed using ImageJ.

Reverse Transcription (RT-) and ATAC-qPCR

For RT-qPCR, total RNA was extracted and purified using the Quick-RNA MiniPrep Kit (Zymo Research). The quantity and quality of RNA was determined using a spectrophotometer. RNA was reverse transcribed using the High-Capacity RNA to cDNA Kit (Applied Biosystems) according to the manufacturer's instructions. For ATAC-qPCR, cells were processed as described above for ATAC-Seq. For qPCR, nuclei were isolated from 50,000 cells and sequencing adapters were transposed for 30 min at 37 °C using 2.5 µl of TDE1 (Nextera Tn5 transposase, Illumina). The reaction was terminated and purified using MinElute reaction cleanup (Qiagen) and used as template. In both cases, qPCR was performed using 1 µl of 5 µM Powerup SYBR green PCR Master Mix (Applied Biosystems), 2 µl of dH$_2$O and 2 µL of cDNA sample in a 10 µl reaction. Each measurement was carried out in a duplicate using a CFX384 Real-Time System (Bio-Rad). The PCR conditions were: 95 °C for 2 min, followed by 40 cycles of 95 °C for 15 s, and 60 °C for 60 s. For ATAC-qPCR, primers were designed to flank the center of the DAR as determined by ATAC-Seq. Primer sequences used are listed in Supplementary Table 2. Gene expression levels were normalized to β-actin, and accessibility changes were normalized to GAPDH.

Affinity purification followed by mass spectrometry (AP-MS)

Nuclear fractionation and AP were performed using the Nuclear Complex Co-IP kit (ActiveMotif) according to manufacturer's instructions. Briefly, cells were trypsinized and washed with cold PBS. The cell pellets were resuspended in hypotonic buffer and incubated on ice for 15 min. Detergent was added and the suspension was centrifuged at for 30 s at 14,000 × *g* in a pre-cooled centrifuge. The nuclear pellet was resuspended in complete digestion buffer with 0.75 µl of enzymatic shearing cocktail and incubated at 37 °C for 10 min. 0.5 M EDTA (3 µl) was added to stop the reaction. The suspension was placed on ice for 5 min and then centrifuged for 10 min at 14,000 × *g*. For AP, the supernatant was pre-cleared by adding 30 µl of Dynabeads Protein G (10004D, ThermoFisher Scientific) and incubated on a rotator at 4 °C for 1 h. The beads were removed and the supernatant was used for subsequent AP. Antibodies (2 µg) targeting either KLF (sc166238, Santa Cruz Biotechnology) or FLAG (F7425, Millipore Sigma) were added per 1 mg of pre-cleared supernatant and incubated on a rotator at 4 °C overnight. The next day, samples were incubated with 30 µl of Dynabeads Protein G (10004D, ThermoFisher Scientific) on a rotator at 4 °C for 1 h. After three successive washes with ice-cold washing buffer, the proteins were eluted from the beads using 100 µl of IgG Elution Buffer (ThermoFisher Scientific) at a gentle vortex at room temperature (RT) for 7 min. The eluate was then immediately neutralized with 1:10 1 M Tris-HCl, pH 8.5. For MS analysis, samples were reduced with 5 mM DTT in 120 µl of 50 mM ammonium bicarbonate. Following reduction, proteins were alkylated using 10 mM acrylamide for 30 min at room temperature to cap cysteines. Digestion was performed using Trypsin/LysC (Promega) overnight at 37 °C. Following digestion and acid quenching, samples were passed over HILIC resin (Resyn Biosciences), dried in a speed vac and then reconstituted in 10 µl reconstitution buffer (2% acetonitrile with 0.1% Formic acid); 3 µl of the reconstituted peptides were injected on the instrument.

All mass spectrometry experiments were performed using an Orbitrap Fusion Tribrid mass spectrometer (ThermoFisher Scientific) with an attach Acquity M-Class UPLC (Waters Corporation) liquid chromatograph. A pulled-and-packed fused silica C18 reverse phase column containing Dr. Maisch 1.8 µm C18 beads and a length of ~25 cm was used over a 80 min gradient. A flow rate of 300 nL/min was used with the mobile phase A consisting of aqueous 0.2% formic acid and mobile phase B consisting of 0.2% formic acid in acetonitrile. Peptides were directly injected onto the analytical column. The mass spectrometer was operated in a data dependent fashion, with MS1 survey spectra collected in the Orbitrap and MS2 fragmentation using CID for in the ion trap.

For data analysis, the raw data files were processed using Byonic v2.14.27 (Protein Metrics) to identify peptides and infer proteins against the human UniProt database containing isoforms concatenated with synthesized sequences. Proteolysis was assumed to be tryptic in nature and allowed for ragged n-terminal digestion and up to two missed cleavage sites. Precursor mass accuracies were held within 12 ppm, with MS/MS fragments held to a 0.4 Da mass accuracy. Proteins were held to a false discovery rate of 1%, using standard approaches.

Proximity ligation assays (PLA)

PLA in cultured PAEC were performed using Duolink PLA protein detection technology (Millipore Sigma) according to manufacturer's instructions. Briefly, slides with PAEC were crosslinked with 4% PFA for

10 min, washed and incubated with Duolink Blocking solution for 1 h at 37 °C. Slides were incubated with rabbit antibodies targeting KLF4 (1:100, sc20691, Santa Cruz Biotechnology) and mouse antibodies targeting BRG1 (1:75, sc17796, Santa Cruz Biotechnology) or SMARCC2 (1:75, sc17838, Santa Cruz Biotechnology) overnight at 4 °C. Rabbit and mouse IgG were used as controls. The next day, slides were washed, and then incubated with the Duolink PLUS and MINUS probes for 1 h at 37 °C. After washing the slides, the probes were ligated for 30 min at 37 °C. Slides were washed and rolling circle amplification was performed for 100 min at 37 °C, after which slides underwent final washes and were mounted using Duolink in situ mounting medium with DAPI (Millipore Sigma). Stained slides were imaged using Leica Application Suite X software on a Leica Sp8 (Leica). Quantification of the average number of foci per nucleus was performed using ImageJ.

For PLA in rat lung tissue, the protocol was modified using longer incubation times to allow reagents to fully penetrate the tissues. Healthy untreated 8-week-old Sprague Dawley rats (n = 2) were sacrificed, and lungs were flushed and perfusion fixed with 4% PFA for 30 min on ice, washed with PBS, and dehydrated in methanol. Following rehydration, tissue was cut in 350 µm thick sections. Sections were bleached using 3% H_2O_2 for 1 h at RT, washed with 0.5% triton-PBS and blocked using 5% DS 5% BSA in 0.5% triton-PBS for 3 h at RT. Sections were incubated with primary antibodies targeting KLF4 (1:50, sc20691, Santa Cruz Biotechnology) and BRG1 (1:30, sc17796, Santa Cruz Biotechnology) in 3% DS 1% BSA in 0.1% triton-PBS overnight at 4 °C. The following day, sections were washed, blocked using 3% DS 1% BSA in 0.1% triton-PBS (dilution buffer) for 4 h at RT, after which they were incubated with the Duolink PLUS and MINUS probes overnight at 4 °C. On the next day, sections were washed, and the probes were ligated for 2 h at 37 °C. After washing, rolling circle amplification was performed for 3 h at 37 °C, after which slides underwent final washes. Sections were post-fixed using 4% PFA for 25 min at RT, washed, and blocked with anti-Rabbit IgG in dilution buffer at RT. Sections were then incubated with FITC-conjugated anti-αSMA antibodies (1:400, F377, Sigma-Aldrich) and antibodies targeting vWF (1:500, ab6994, Abcam) overnight at 4 °C. After washing, sections were incubated with anti-Rabbit Alexa Fluor 647-conjugated secondary antibodies (1:200, A32795, Thermo Fisher Scientific) for 3 h at RT, washed in triton-PBS with DAPI for 2 h at RT, and post-fixed with 4% PFA for 30 min at RT. Finally, sections were washed, dehydrated in methanol, and cleared using Benzyl Alcohol/ Benzyl Benzoate (BABB). Sections were imaged using Leica Application Suite X software on a Leica Sp8 (Leica). Three-dimensional reconstructions were made with Imaris version 9.3.0 (Bitplane).

H3K27ac HiC chromatin immunoprecipitation (HiChIP)

H3K27ac HiChIP was performed as previously described[19]. PAEC were crosslinked in 1% formaldehyde for 10 min at room temperature and then quenched by 125 mM Glycine for 5 min at RT. Nuclei were isolated from 1 million crosslinked cells by 30 min of lysis at 4 °C. Nuclei were permeabilized in 0.5% SDS for 10 min at 62 °C and quenched using Triton X-100 for 15 min at 37 °C. MboI restriction enzyme (R0147, New England Biolabs) was added to digest chromatin for 2 h at 37 °C and then heat-inactivated for 20 min at 62 °C. Klenow was then used to fill in restriction fragment overhangs and mark the DNA ends with biotin (M0210, New England Biolabs). Proximity ligation contact (PLC) pellets were then created by incubation with DNA ligase for 4 h at room temperature followed by centrifugation. PLC pellets were then sonicated and immunoprecipitated using 5 µg of H3K27ac antibodies (#8173, Cell signaling Technology) as previously described. The eluted fragments labeled by biotin were then captured by streptavidin bead pull-down. DNA was then adaptor-labeled using Tn5 transposase (Illumina) and subjected to PCR amplification. Samples were then sequenced by 2 × 101 paired-end sequencing on an Illumina NovaSeq 6000 to an average yield of 200 million reads per sample

(Supplementary Table 1). The resulting data were filtered for duplicate reads, aligned to the hg19 genome, and filtered for valid interactions using the HiC-Pro pipeline v.2.11.1 (https://github.com/nservant/HiC-Pro) using the default settings. FitHiChIP (https://github.com/ay-lab/FitHiChIP) was used to determine statistically significant interactions using default settings, with the exception of allowing interactions with a minimum size of 1Kb. The diffLoop package (https://github.com/aryeelab/diffloop) was used to test for differential interactions between conditions, and to infer gene enhancer to promoter relationships.

Activity-by-contact model (ABC)

The ABC v0.2 pipeline was cloned from the GitHub repository (https://github.com/broadinstitute/ABC-Enhancer-Gene-Prediction/). First, ATAC peaks were called by MACS2 v.2.1.2 (https://github.com/taoliu/MACS) from each ATAC BAM file with a P-value cutoff of 0.1. Candidate enhancer regions were then defined by the ABC script makeCandidateRegions.py, which: (1) Resized each peak to be 250 base pairs centered on the peak summit. (2) Counted ATAC-seq reads in each peak and retained the top 150,000 peaks with the most read counts. (3) Removed any regions that are blacklisted due to known propensity for errors (hg19-blacklist.v2.bed from https://github.com/Boyle-Lab/Blacklist) and (4), merged any overlapping regions. Enhancer activity was then quantified by the ABC script run.neighborhoods.py, which counted ATAC-seq and H3K27ac ChIP-seq reads in the candidate enhancer regions that were generated in the previous step, gene bodies, and promoter regions. Lastly, the ABC score was calculated using the ABC script predict.py; which combined information from the enhancer and promoter activities, calculated in the previous step, with contact frequency data from average Hi-C profiles of 10 cell lines (ftp://ftp.broadinstitute.org/outgoing/lincRNA/average_hic/average_hic.v2.191020.tar.gz. The default threshold of 0.02 was applied which corresponds to approximately 70% recall and 60% precision[21].

CRISPR-interference

PAEC were transduced with a lentiviral vector encoding a doxycylin-inducible mutant of a catalytically dead Cas9 fused to the bipartite repressor domain MeCP2-KRAB, as described above. Cells were treated with 500 ng/µl of doxycycline 48 h prior to nucleofection of synthetic guide RNAs (sgRNA) (Synthego) using the Basic Nucleofector Kit for Primary Mammalian Endothelial Cells (Lonza). sgRNA were designed to target the KLF binding sites in the candidate enhancers using the GPP sgRNA Design tool from the Broad Institute (https://portals.broadinstitute.org/gpp/public/analysis-tools/sgrna-design). The sequences used are listed in Supplementary Table 2. Cells were allowed to recover for 24 h and then exposed to 24 h of LSS, after which target gene expression was assessed by RT-qPCR.

Statistical analysis

Values from multiple experiments are shown as arithmetical mean ± SEM. Statistical significance was determined using unpaired two-tailed Student's t test. Correlations were calculated by Pearson R test. A P-value of <0.05 was considered significant. The number of samples in each group, the statistical test used, and the statistical significance is indicated in the figures. Data were analyzed using Prism version 8.4 (Graphpad).

Reporting summary

Further information on research design is available in the Nature Research Reporting Summary linked to this article.

Data availability

The data that support this study are available from the corresponding author upon reasonable request. ATAC-Seq, RNA-Seq, ChIP-seq and HiChIP data are deposited in the Gene Expression Omnibus (GEO)

under accession number GSE152900. AP-MS data is deposited in MassIVE under accession number MSV000085825. Source data are provided with this paper.

References

1. Friedman, M. H., Bargeron, C. B., Deters, O. J., Hutchins, G. M. & Mark, F. F. Correlation between wall shear and intimal thickness at a coronary artery branch. *Atherosclerosis* **68**, 27–33 (1987).
2. Ku, D. N., Giddens, D. P., Zarins, C. K. & Glagov, S. Pulsatile flow and atherosclerosis in the human carotid bifurcation. Positive correlation between plaque location and low oscillating shear stress. *Arteriosclerosis* **5**, 293–302 (1985).
3. Cybulsky, M. I. & Gimbrone, M. A. Jr. Endothelial expression of a mononuclear leukocyte adhesion molecule during atherogenesis. *Science* **251**, 788–791 (1991).
4. Davies, P. F., Civelek, M., Fang, Y. & Fleming, I. The atherosusceptible endothelium: Endothelial phenotypes in complex haemodynamic shear stress regions in vivo. *Cardiovasc Res* **99**, 315–327 (2013).
5. Malek, A. M., Alper, S. L. & Izumo, S. Hemodynamic shear stress and its role in atherosclerosis. *JAMA* **282**, 2035–2042 (1999).
6. Tzima, E. et al. A mechanosensory complex that mediates the endothelial cell response to fluid shear stress. *Nature* **437**, 426–431 (2005).
7. Hahn, C. & Schwartz, M. A. Mechanotransduction in vascular physiology and atherogenesis. *Nat. Rev. Mol. Cell Biol.* **10**, 53–62 (2009).
8. Davies, P. F. Flow-mediated endothelial mechanotransduction. *Physiol. Rev.* **75**, 519–560 (1995).
9. Dekker, R. J. et al. Prolonged fluid shear stress induces a distinct set of endothelial cell genes, most specifically lung Kruppel-like factor (KLF2). *Blood* **100**, 1689–1698 (2002).
10. Parmar, K. M. et al. Integration of flow-dependent endothelial phenotypes by Kruppel-like factor 2. *J. Clin. Invest.* **116**, 49–58 (2006).
11. Hamik, A. et al. Kruppel-like factor 4 regulates endothelial inflammation. *J. Biol. Chem.* **282**, 13769–13779 (2007).
12. Villarreal, G. Jr. et al. Defining the regulation of KLF4 expression and its downstream transcriptional targets in vascular endothelial cells. *Biochem. Biophys. Res. Commun.* **391**, 984–989 (2010).
13. Sangwung, P. et al. KLF2 and KLF4 control endothelial identity and vascular integrity. *JCI Insight* **2**, e91700 (2017).
14. Pietra, G. G. et al. Histopathology of primary pulmonary hypertension. A qualitative and quantitative study of pulmonary blood vessels from 58 patients in the National Heart, Lung, and Blood Institute, Primary Pulmonary Hypertension Registry. *Circulation* **80**, 1198–1206 (1989).
15. Rabinovitch, M. Molecular pathogenesis of pulmonary arterial hypertension. *J. Clin. Invest.* **122**, 4306–4313 (2012).
16. Deng, Z. et al. Familial primary pulmonary hypertension (gene PPH1) is caused by mutations in the bone morphogenetic protein receptor-II gene. *Am. J. Hum. Genet.* **67**, 737–744 (2000).
17. Lane, K. B. et al. Heterozygous germline mutations in BMPR2, encoding a TGF-beta receptor, cause familial primary pulmonary hypertension. *Nat. Genet.* **26**, 81–84 (2000).
18. Gupta, R. M. et al. A genetic variant associated with five vascular diseases is a distal regulator of endothelin-1 gene expression. *Cell* **170**, 522–533.e515 (2017).
19. Mumbach, M. R. et al. HiChIP: efficient and sensitive analysis of protein-directed genome architecture. *Nat. Methods* **13**, 919–922 (2016).
20. Mumbach, M. R. et al. Enhancer connectome in primary human cells identifies target genes of disease-associated DNA elements. *Nat. Genet.* **49**, 1602–1612 (2017).
21. Fulco, C. P. et al. Activity-by-contact model of enhancer-promoter regulation from thousands of CRISPR perturbations. *Nat. Genet.* **51**, 1664–1669 (2019).
22. Tang, B. T. et al. Wall shear stress is decreased in the pulmonary arteries of patients with pulmonary arterial hypertension: An image-based, computational fluid dynamics study. *Pulm. Circ.* **2**, 470–476 (2012).
23. McLaughlin, F. et al. Combined genomic and antisense analysis reveals that the transcription factor Erg is implicated in endothelial cell differentiation. *Blood* **98**, 3332–3339 (2001).
24. De Val, S. et al. Combinatorial regulation of endothelial gene expression by ets and forkhead transcription factors. *Cell* **135**, 1053–1064 (2008).
25. Fledderus, J. O. et al. Prolonged shear stress and KLF2 suppress constitutive proinflammatory transcription through inhibition of ATF2. *Blood* **109**, 4249–4257 (2007).
26. Qiao, C. et al. Deep transcriptomic profiling reveals the similarity between endothelial cells cultured under static and oscillatory shear stress conditions. *Physiol. Genomics* **48**, 660–666 (2016).
27. Ohnesorge, N. et al. Erk5 activation elicits a vasoprotective endothelial phenotype via induction of Kruppel-like factor 4 (KLF4). *J. Biol. Chem.* **285**, 26199–26210 (2010).
28. Moonen, J. R. et al. Endothelial-to-mesenchymal transition contributes to fibro-proliferative vascular disease and is modulated by fluid shear stress. *Cardiovasc. Res.* **108**, 377–386 (2015).
29. Mandl, M., Slack, D. N. & Keyse, S. M. Specific inactivation and nuclear anchoring of extracellular signal-regulated kinase 2 by the inducible dual-specificity protein phosphatase DUSP5. *Mol. Cell Biol.* **25**, 1830–1845 (2005).
30. Bhattacharyya, S., Chandra, V., Vijayanand, P. & Ay, F. Identification of significant chromatin contacts from HiChIP data by FitHiChIP. *Nat. Commun.* **10**, 4221 (2019).
31. Giaid, A. et al. Expression of endothelin-1 in the lungs of patients with pulmonary hypertension. *N. Engl. J. Med.* **328**, 1732–1739 (1993).
32. Channick, R. N. et al. Effects of the dual endothelin-receptor antagonist bosentan in patients with pulmonary hypertension: A randomised placebo-controlled study. *Lancet* **358**, 1119–1123 (2001).
33. Salmon, M., Gomez, D., Greene, E., Shankman, L. & Owens, G. K. Cooperative binding of KLF4, pELK-1, and HDAC2 to a G/C repressor element in the SM22alpha promoter mediates transcriptional silencing during SMC phenotypic switching in vivo. *Circ. Res.* **111**, 685–696 (2012).
34. Yeo, N. C. et al. An enhanced CRISPR repressor for targeted mammalian gene regulation. *Nat. Methods* **8**, 611–616 (2018).
35. Fang, J. S. et al. Shear-induced Notch-Cx37-p27 axis arrests endothelial cell cycle to enable arterial specification. *Nat. Commun.* **8**, 2149 (2017).
36. Maurano, M. T. et al. Systematic localization of common disease-associated variation in regulatory DNA. *Science* **337**, 1190–1195 (2012).
37. Evangelou, E. et al. Genetic analysis of over 1 million people identifies 535 new loci associated with blood pressure traits. *Nat. Genet.* **50**, 1412–1425 (2018).
38. The Coronary Artery Disease (C4D) Genetics Consortium. A genome-wide association study in Europeans and South Asians identifies five new loci for coronary artery disease. *Nat. Genet.* **43**, 339–344 (2011).
39. Erdmann, J. et al. Genome-wide association study identifies a new locus for coronary artery disease on chromosome 10p11.23. *Eur. Heart J.* **32**, 158–168 (2011).
40. Douglas, G. et al. A key role for the novel coronary artery disease gene JCAD in atherosclerosis via shear stress mechanotransduction. *Cardiovasc. Res.* **116**, 1863–1874 (2020).

41. Salvi, E. et al. Genomewide association study using a high-density single nucleotide polymorphism array and case-control design identifies a novel essential hypertension susceptibility locus in the promoter region of endothelial NO synthase. *Hypertension* **59**, 248–255 (2012).

42. Luizon, M. R., Metzger, I. F., Lacchini, R. & Tanus-Santos, J. E. Endothelial nitric oxide synthase polymorphism rs3918226 associated with hypertension does not affect plasma nitrite levels in healthy subjects. *Hypertension* **59**, e52 (2012).

43. Kim, K. M. et al. Molecular characterization of myosin phosphatase in endothelium. *J. Cell Physiol.* **227**, 1701–1708 (2012).

44. Illi, B. et al. Shear stress-mediated chromatin remodeling provides molecular basis for flow-dependent regulation of gene expression. *Circ. Res.* **93**, 155–161 (2003).

45. Chen, W., Bacanamwo, M. & Harrison, D. G. Activation of p300 histone acetyltransferase activity is an early endothelial response to laminar shear stress and is essential for stimulation of endothelial nitric-oxide synthase mRNA transcription. *J. Biol. Chem.* **283**, 16293–16298 (2008).

46. Chen, Z. et al. Shear stress, SIRT1, and vascular homeostasis. *Proc. Natl Acad. Sci. USA* **107**, 10268–10273 (2010).

47. Zampetaki, A. et al. Histone deacetylase 3 is critical in endothelial survival and atherosclerosis development in response to disturbed flow. *Circulation* **121**, 132–142 (2010).

48. Lee, D. Y. et al. Role of histone deacetylases in transcription factor regulation and cell cycle modulation in endothelial cells in response to disturbed flow. *Proc. Natl Acad. Sci. USA* **109**, 1967–1972 (2012).

49. Maleszewska, M., Vanchin, B., Harmsen, M. C. & Krenning, G. The decrease in histone methyltransferase EZH2 in response to fluid shear stress alters endothelial gene expression and promotes quiescence. *Angiogenesis* **19**, 9–24 (2016).

50. Dunn, J. et al. Flow-dependent epigenetic DNA methylation regulates endothelial gene expression and atherosclerosis. *J. Clin. Invest.* **124**, 3187–3199 (2014).

51. Zhou, J., Li, Y. S., Wang, K. C. & Chien, S. Epigenetic mechanism in regulation of endothelial function by disturbed flow: Induction of DNA hypermethylation by DNMT1. *Cell Mol. Bioeng.* **7**, 218–224 (2014).

52. Jiang, Y. Z., Manduchi, E., Stoeckert, C. J. Jr. & Davies, P. F. Arterial endothelial methylome: Differential DNA methylation in athero-susceptible disturbed flow regions in vivo. *BMC Genomics* **16**, 506 (2015).

53. He, M. et al. Atheroprotective flow upregulates ITPR3 (inositol 1,4,5-trisphosphate receptor 3) in vascular endothelium via KLF4 (Kruppel-like factor 4)-mediated histone modifications. *Arterioscler. Thromb. Vasc. Biol.* **39**, 902–914 (2019).

54. Kumar, S., Kim, C. W., Simmons, R. D. & Jo, H. Role of flow-sensitive microRNAs in endothelial dysfunction and atherosclerosis: mechanosensitive athero-miRs. *Arterioscler. Thromb. Vasc. Biol.* **34**, 2206–2216 (2014).

55. Wu, W. et al. Flow-dependent regulation of Kruppel-like factor 2 is mediated by MicroRNA-92a. *Circulation* **124**, 633–641 (2011).

56. Fang, Y. & Davies, P. F. Site-specific microRNA-92a regulation of Kruppel-like factors 4 and 2 in atherosusceptible endothelium. *Arterioscler. Thromb. Vasc. Biol.* **32**, 979–987 (2012).

57. Man, H. S. J. et al. Angiogenic patterning by STEEL, an endothelial-enriched long noncoding RNA. *Proc. Natl Acad. Sci. USA* **115**, 2401–2406 (2018).

58. Miao, Y. et al. Enhancer-associated long non-coding RNA LEENE regulates endothelial nitric oxide synthase and endothelial function. *Nat. Commun.* **9**, 292 (2018).

59. Orphanides, G., Lagrange, T. & Reinberg, D. The general transcription factors of RNA polymerase II. *Genes Dev.* **10**, 2657–2683 (1996).

60. Banerji, J., Rusconi, S. & Schaffner, W. Expression of a beta-globin gene is enhanced by remote SV40 DNA sequences. *Cell* **27**, 299–308 (1981).

61. Osterwalder, M. et al. Enhancer redundancy provides phenotypic robustness in mammalian development. *Nature* **554**, 239–243 (2018).

62. Reyes-Palomares, A. et al. Remodeling of active endothelial enhancers is associated with aberrant gene-regulatory networks in pulmonary arterial hypertension. *Nat. Commun.* **11**, 1673 (2020).

63. Kim, M. et al. Laminar flow activation of ERK5 protein in vascular endothelium leads to atheroprotective effect via NF-E2-related factor 2 (Nrf2) activation. *J. Biol. Chem.* **287**, 40722–40731 (2012).

64. Skene, P.J. & Henikoff, S. An efficient targeted nuclease strategy for high-resolution mapping of DNA binding sites. *Elife* **6**, e2185 (2017).

65. Takahashi, K. & Yamanaka, S. Induction of pluripotent stem cells from mouse embryonic and adult fibroblast cultures by defined factors. *Cell* **126**, 663–676 (2006).

66. Iwafuchi-Doi, M. & Zaret, K. S. Pioneer transcription factors in cell reprogramming. *Genes Dev.* **28**, 2679–2692 (2014).

67. Soufi, A. et al. Pioneer transcription factors target partial DNA motifs on nucleosomes to initiate reprogramming. *Cell* **161**, 555–568 (2015).

68. Soufi, A., Donahue, G. & Zaret, K. S. Facilitators and impediments of the pluripotency reprogramming factors' initial engagement with the genome. *Cell* **151**, 994–1004 (2012).

69. Kwon, H., Imbalzano, A. N., Khavari, P. A., Kingston, R. E. & Green, M. R. Nucleosome disruption and enhancement of activator binding by a human SW1/SNF complex. *Nature* **370**, 477–481 (1994).

70. Kingston, R. E. & Narlikar, G. J. ATP-dependent remodeling and acetylation as regulators of chromatin fluidity. *Genes Dev.* **13**, 2339–2352 (1999).

71. Burns, L. G. & Peterson, C. L. The yeast SWI-SNF complex facilitates binding of a transcriptional activator to nucleosomal sites in vivo. *Mol. Cell Biol.* **17**, 4811–4819 (1997).

72. Cosma, M. P., Tanaka, T. & Nasmyth, K. Ordered recruitment of transcription and chromatin remodeling factors to a cell cycle- and developmentally regulated promoter. *Cell* **97**, 299–311 (1999).

73. Ryan, M. P., Jones, R. & Morse, R. H. SWI-SNF complex participation in transcriptional activation at a step subsequent to activator binding. *Mol. Cell Biol.* **18**, 1774–1782 (1998).

74. Li, Z. et al. Foxa2 and H2A.Z mediate nucleosome depletion during embryonic stem cell differentiation. *Cell* **151**, 1608–1616 (2012).

75. Khavari, P. A., Peterson, C. L., Tamkun, J. W., Mendel, D. B. & Crabtree, G. R. BRG1 contains a conserved domain of the SWI2/SNF2 family necessary for normal mitotic growth and transcription. *Nature* **366**, 170–174 (1993).

76. Chronis, C. et al. Cooperative binding of transcription factors orchestrates reprogramming. *Cell* **168**, 442–459.e420 (2017).

77. Alver, B. H. et al. The SWI/SNF chromatin remodelling complex is required for maintenance of lineage specific enhancers. *Nat. Commun.* **8**, 14648 (2017).

78. Kidder, B. L., Palmer, S. & Knott, J. G. SWI/SNF-Brg1 regulates self-renewal and occupies core pluripotency-related genes in embryonic stem cells. *Stem Cells* **27**, 317–328 (2009).

79. Mak, A. B. et al. A lentiviral functional proteomics approach identifies chromatin remodeling complexes important for the induction of pluripotency. *Mol. Cell Proteom.* **9**, 811–823 (2010).

80. Dekker, J., Rippe, K., Dekker, M. & Kleckner, N. Capturing chromosome conformation. *Science* **295**, 1306–1311 (2002).

81. Lieberman-Aiden, E. et al. Comprehensive mapping of long-range interactions reveals folding principles of the human genome. *Science* **326**, 289–293 (2009).

82. Rao, S. S. et al. A 3D map of the human genome at kilobase resolution reveals principles of chromatin looping. *Cell* **159**, 1665–1680 (2014).

83. Di Giammartino, D. C. et al. KLF4 is involved in the organization and regulation of pluripotency-associated three-dimensional enhancer networks. *Nat. Cell Biol.* **21**, 1179–1190 (2019).

84. Dixit, A. et al. Perturb-Seq: Dissecting molecular circuits with scalable single-cell RNA profiling of pooled genetic screens. *Cell* **167**, 1853–1866.e1817 (2016).

85. Buenrostro, J. D. et al. Transposition of native chromatin for fast and sensitive epigenomic profiling of open chromatin, DNA-binding proteins, and nucleosome position. *Nat. Methods* **10**, 1213–1218 (2013).

Acknowledgements

Author contributions

J.-R.M., J.C., M.P.S., and M.R. conceived the project and designed the research studies. J.-R.M and J.C. performed the experiments and analyzed the data. M.S. and D.L. provided technical assistance with the ChIP-Seq studies. T.S. performed RT-qPCR analyses. M.R.M., H.Y.C., and R.V.N. assisted with the HiChIP studies. F.Z. and R.J.M. assisted with the tissue imaging studies. J.N. and J.M.E. assisted with the ABC algorithm. D.H.M. assisted with the in vitro PLA studies. S.T. assisted with cell cultures. L.W. assisted with preparing tissues for imaging. J.-R.M. and M.R. prepared the manuscript.

Competing interests

The authors declare no competing interests.

Additional information